Protein arginine methyltransferase CARM1 attenuates the paraspeckle-mediated nuclear retention of mRNAs containing IR*Alu*s

Shi-Bin Hu,[1] Jian-Feng Xiang,[1] Xiang Li,[1] Yefen Xu,[1] Wei Xue,[2] Min Huang,[1] Catharine C. Wong,[1] Cari A. Sagum,[3] Mark T. Bedford,[3] Li Yang,[2,4] Donghang Cheng,[3] and Ling-Ling Chen[1,4]

[1]State Key Laboratory of Molecular Biology, Institute of Biochemistry and Cell Biology, Shanghai Institutes for Biological Sciences, Chinese Academy of Sciences, Shanghai 200031, China; [2]Key Laboratory of Computational Biology, Chinese Academy of Sciences (CAS)-German Max Planck Society (MPG) Partner Institute for Computational Biology, Shanghai Institutes for Biological Sciences, Chinese Academy of Sciences, Shanghai 200031, China; [3]The University of Texas M.D. Anderson Cancer Center, Smithville, Texas 78957, USA; [4]School of Life Science and Technology, ShanghaiTech University, Shanghai 200031, China

In many cells, mRNAs containing inverted repeated *Alu* elements (IR*Alu*s) in their 3′ untranslated regions (UTRs) are inefficiently exported to the cytoplasm. Such nuclear retention correlates with paraspeckle-associated protein complexes containing p54^{nrb}. However, nuclear retention of mRNAs containing IR*Alu*s is variable, and how regulation of retention and export is achieved is poorly understood. Here we show one mechanism of such regulation via the arginine methyltransferase CARM1 (coactivator-associated arginine methyltransferase 1). We demonstrate that disruption of CARM1 enhances the nuclear retention of mRNAs containing IR*Alu*s. CARM1 regulates this nuclear retention pathway at two levels: CARM1 methylates the coiled-coil domain of p54^{nrb}, resulting in reduced binding of p54^{nrb} to mRNAs containing IR*Alu*s, and also acts as a transcription regulator to suppress *NEAT1* transcription, leading to reduced paraspeckle formation. These actions of CARM1 work together synergistically to regulate the export of transcripts containing IR*Alu*s from paraspeckles under certain cellular stresses, such as poly(I:C) treatment. This work demonstrates how a post-translational modification of an RNA-binding protein affects protein–RNA interaction and also uncovers a mechanism of transcriptional regulation of the long noncoding RNA *NEAT1*.

[*Keywords*: paraspeckles; p54^{nrb}; nuclear retention; CARM1; *NEAT1*]

Supplemental material is available for this article.

Received December 8, 2014; revised version accepted February 13, 2015.

The mammalian nucleus is highly organized into chromosome territories and a number of distinct membrane-less nuclear bodies or subnuclear structures that can affect nuclear neighborhoods and gene regulation (Zhao et al. 2009). Distinct nuclear bodies contain specific protein and RNA components that define particular nuclear processes (Mao et al. 2011b).

Paraspeckles, first identified in 2002 (Fox et al. 2002), are composed of the long noncoding RNA (lncRNA) *NEAT1*, which confers structural integrity and multiple proteins for its potential functions (Prasanth et al. 2005; Chen et al. 2008; Chen and Carmichael 2009; Clemson et al. 2009; Sasaki et al. 2009; Sunwoo et al. 2009; Naganuma et al. 2012). There are two isoforms of *NEAT1* lncRNAs, *NEAT1_v1* and *NEAT1_v2*, produced by alternative 3′ end processing (Naganuma et al. 2012). A live-cell imaging system aiming to visualize the inducible transcription of *NEAT1* lncRNAs and paraspeckle proteins revealed that both the active transcription of *NEAT1* and *NEAT1* lncRNAs regulate paraspeckle maintenance and dynamics (Mao et al. 2011a). In addition to several well-studied *Drosophila* behavior and human splicing (DBHS) family proteins (including PSP1α, p54^{nrb}, and PSF, which were known to be localized to paraspeckles) (Fox et al. 2002, 2005; Bond and Fox 2009), new paraspeckle proteins (including many RNA-binding

Corresponding authors: linglingchen@sibcb.ac.cn, dcheng@mdanderson.org
Article is online at http://www.genesdev.org/cgi/doi/10.1101/gad.257048.114.

proteins) were recently identified (Naganuma et al. 2012; West et al. 2014).

Recent studies have revealed that both *NEAT1* lncRNAs and paraspeckle proteins can mediate the function of paraspeckles in gene regulation, although the detailed mechanisms remain to be fully defined. For example, the abundant *NEAT1* RNA was shown to regulate transcription by sequestrating the paraspeckle protein PSF (Hirose et al. 2014; Imamura et al. 2014). Such sequestration of the transcriptional repressor PSF resulted in the activation of IL8 expression upon immune stimuli (Imamura et al. 2014) and *ADARB2* transcription (Hirose et al. 2014). Moreover, genome-wide analyses recently revealed that *NEAT1* can associate with hundreds of active chromatin sites (West et al. 2014), consistent with the view that paraspeckles may be involved in transcription regulation.

In addition to *NEAT1*-mediated regulation, $p54^{nrb}$ is involved in the paraspeckle-mediated nuclear retention of mRNAs containing inverted repeats in their 3′ untranslated regions (UTRs) (Prasanth et al. 2005; Chen et al. 2008; Chen and Carmichael 2009; Mao et al. 2011a; Elbarbary et al. 2013). The mouse *CTN-RNA*, which contains a dsRNA structure resulting from inverted short interspersed nuclear elements (SINEs) in its 3′ UTR, is retained in the nucleus and at least partially localized to paraspeckles (Prasanth et al. 2005). In human cells, hundreds of genes contain inverted repeated SINEs (mainly *Alu* elements) in their 3′ UTRs. *Alu* elements are unique to primates and account for almost all of the human SINEs and >10% of the genome. Their abundance leads to the frequent occurrence of inverted repeat structures (inverted repeated *Alu* elements [IR*Alu*s]) in gene regions (Chen and Carmichael 2008). We reported previously that mRNAs containing IR*Alu*s in their 3′ UTRs are retained in the nucleus in paraspeckles and in association with $p54^{nrb}$ (Chen et al. 2008; Chen and Carmichael 2009). Such regulation at paraspeckles in human cells was further demonstrated by live-cell imaging (Mao et al. 2011a). Therefore, this nuclear retention pathway of IR*Alu*s in 3′ UTRs of genes provides an additional layer of gene regulation by sequestering otherwise mature mRNAs within the nucleus.

Interestingly, we and others observed that the nuclear retention of transcripts containing IR*Alu*s is variable, with some such mRNAs located in the nucleus, while others are in the cytoplasm (Chen and Carmichael 2008; Chen et al. 2008; Hundley et al. 2008; Elbarbary et al. 2013). How is such nuclear retention of mRNAs containing IR*Alu*s at paraspeckles achieved and regulated? Earlier observations suggested that the mouse *CTN-RNA* is retained in the nucleus until cell stress occurs, resulting in the cleavage and removal of its 3′ UTR nuclear retention signal (inverted repeats of murine SINEs) by an unknown mechanism. The truncated message is then transported efficiently to the cytoplasm for translation (Prasanth et al. 2005). However, some mRNAs containing IR*Alu*s were seen in the cytoplasm (Chen et al. 2008; Hundley et al. 2008; Elbarbary et al. 2013), implying that other mechanisms may be involved in the release of paraspeckle-mediated nuclear retention of mRNAs containing IR*Alu*s. For instance, it had been shown recently that the dsRNA-binding protein Staufen 1 competed with $p54^{nrb}$ for the binding to 3′ UTR IR*Alu*s, resulting in an enhanced nuclear export and translation of these RNAs (Elbarbary et al. 2013). Another hypothesis is that post-translational modifications on $p54^{nrb}$ could alter its binding activity to mRNAs containing IR*Alu*s.

CARM1 (coactivator-associated arginine methyltransferase), also known as PRMT4, was the first identified nuclear receptor coactivator in a family of nine PRMT members (PRMT1–9) (Bedford and Clarke 2009). CARM1 methylates histone H3 at Arg17, generating a docking site for the recruitment of the methylarginine effector TDRD3 (Yang et al. 2010). CARM1 also methylates many nonhistone proteins that play important roles in a number of biological processes, including transcriptional regulation (Chen et al. 1999), mRNA splicing (Cheng et al. 2007), muscle differentiation (Chen et al. 2002), adipocyte differentiation (Yadav et al. 2008), and T-cell development (Li et al. 2013).

Here we describe a new mechanism of gene regulation by CARM1. Disruption of CARM1 significantly enhances the nuclear retention of mRNAs containing IR*Alu*s. We demonstrate that CARM1 regulates the nuclear retention of mRNAs containing IR*Alu*s in paraspeckles at two levels. On the one hand, CARM1 methylates $p54^{nrb}$, resulting in the reduced binding capability to mRNAs containing IR*Alu*s; on the other hand, CARM1 suppresses *NEAT1* transcription and paraspeckle formation. Actions of CARM1 at these two levels synergistically work together to regulate the export of transcripts containing IR*Alu*s from paraspeckles under certain cellular stresses, such as poly(I:C) treatment. This represents one of a few examples where post-translational modification of an RNA-binding protein affects protein–RNA interaction and gene regulation. In addition, it shows how transcriptional regulation of the lncRNA *NEAT1* can occur.

Results

$p54^{nrb}$ is methylated by CARM1

Very few substrates for CARM1 have been characterized, which limits the understanding of the roles of this enzyme. The identification of the repertoire of substrates for CARM1 is an essential step toward a complete understanding of its biological functions. CARM1 substrates are methylated in wild-type mouse embryonic fibroblast (MEF) cells but remain unmethylated in CARM1 knockout cells. Thus, the CARM1 knockout nuclear extracts are good substrates for in vitro methylation assays that would allow the identification of additional CARM1 substrates. We performed in vitro methylation assays using acid-extracted histones from the nuclei of wild-type and $CARM1^{-/-}$ MEFs as substrates and GST-CARM1 as an enzyme. The reaction mixtures were then run on an SDS-PAGE gel, and the indicated protein bands corresponding to potential CARM1 substrates were used for trypsin digestion and subsequent mass spectrometry (MS). Of

the six identified substrates found in duplicated experiments, PABP1 (Lee and Bedford 2002) and SmB (Cheng et al. 2007) were previously described as CARM1 substrates. Interestingly, p54^{nrb}, the well-known paraspeckle component, was also identified as a new CARM1 substrate and was chosen for further study (Fig. 1A).

p54^{nrb} as a substrate of CARM1 was further validated by CARM1 in vitro methylation of *Escherichia coli*-expressed histidine-tagged p54^{nrb} (Fig. 1B). Furthermore, a pan-screening for the activity of arginine methylase family members on p54^{nrb} revealed that PRMT1 and PRMT6 could also methylate p54^{nrb}, but the reaction of CARM1 on p54^{nrb} was the strongest (Supplemental Fig. S1A). Moreover, the in vitro methylation of p54^{nrb} truncations revealed that multiple arginine methylation sites on p54^{nrb} were enriched in the coiled-coil domain and the C-terminal region of the protein (Supplemental Fig. S1B).

To identify the specific methylation sites catalyzed by CARM1, we developed CARM1 knockdown HeLa and HEK293 cell lines (Supplemental Fig. S2A). Flag-tagged p54^{nrb} was expressed in scramble shRNA-treated (scramble) and CARM1 shRNA-treated (CARM1 knockdown) cell lines, and then immunoprecipitation by anti-Flag was performed (Supplemental Fig. S2B) followed by MS analysis. Multiple methylation sites in p54^{nrb} were identified from MS (Supplemental Fig. S2C). Among these sites, R357, R365, and R378 were present in the anti-Flag precipitated complex in scramble cell lines but little in CARM1 knockdown cell lines (Supplemental Fig. S2D; data not shown), confirming that they are CARM1-methylated sites on p54^{nrb}. In vitro methylation assays of p54^{nrb} mutants in which these arginines were replaced with lysines further confirmed that R357, R365, and R378 were the major sites methylated by CARM1 (Fig. 1C).

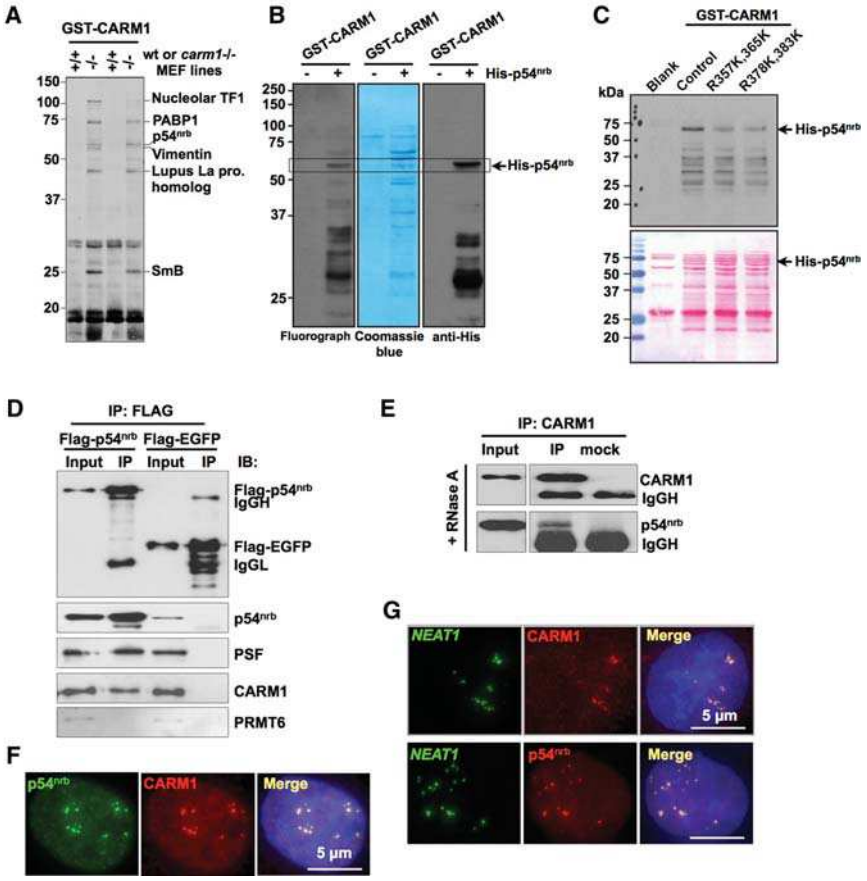

Figure 1. p54^{nrb} is methylated by CARM1. (*A*) p54^{nrb} is a CARM1 substrate. Acid-extracted histones from CARM1 wild-type (wt; +/+) and knockout (–/–) MEFs were used as substrates, and GST-CARM1 was used as an enzyme to perform standard in vitro methylation assays. Reactions were done in duplicate, separated on SDS-PAGE, and transferred to PVDF membranes for fluorography and Ruby staining. The indicated methylated proteins were processed for protein identification using MS. (*B*) p54^{nrb} is methylated in vitro by recombinant CARM1. In vitro methylation reactions were performed using recombinant His-tagged p54^{nrb} with recombinant GST-CARM1 in the presence of [^{3}H]AdoMet. Reactions were separated on SDS-PAGE and transferred to PVDF membranes for fluorography, Coomassie blue gel staining, and immunoblotting with anti-His antibody. (*C*) Lysine replacement of Arg357 and Arg365 (R357K, 365K) and of Arg378 and Arg383 (R378K, 383K) reduces p54^{nrb} methylation. Mutants of p54^{nrb} were made as indicated by MS results and expressed as His-tagged fusion proteins. Purified His-p54^{nrb} mutants were incubated with GST-CARM1 in the presence of [^{3}H]AdoMet. Methylated proteins were separated by SDS-PAGE and visualized by fluorography. The same membrane was subjected to Ponceau staining to verify equal loading. Note that R383 was not identified by MS but was included in the mutation assay. (*D*) p54^{nrb} interacts with CARM1. HeLa cells expressing Flag-p54^{nrb} or Flag-EGFP (control) were immunoprecipitated with anti-Flag antibody and then immunoblotted with anti-Flag, anti-p54^{nrb}, anti-PSF, anti-CARM1, and anti-PRMT6. Note that p54^{nrb} specifically interacted with CARM1 but not PRMT6 in vivo. (IgGH) IgG heavy chain; (IgGL) IgG light chain. (*E*) RNA-independent interaction of p54^{nrb} and CARM1 in HeLa cells. Total extracts of HeLa cells treated with RNase A were immunoprecipitated with CARM1 antibody or mock antibody and then immunoblotted with anti-CARM1 and anti-p54^{nrb}. (*F*) p54^{nrb} and CARM1 colocalize in HeLa cells. HeLa cells were stained with anti-p54^{nrb} and anti-CARM1 antibodies. DAPI was used to indicate DNA. (*G*) CARM1 is a new component of paraspeckles. RNA in situ hybridization (ISH) was performed with digoxigenin (Dig)-labeled antisense *NEAT1* probe (green) in HeLa cells, and representative images are shown. CARM1 and p54^{nrb} are in red. *NEAT1* colocalizes with CARM1 (*top* panels) and p54^{nrb} (*bottom* panels).

The coimmunoprecipitation (co-IP) assays between p54^{nrb} and CARM1 performed in HeLa (Fig. 1D,E) and HEK293 (data not shown) cells both revealed that they interacted with each other endogenously. CARM1 was detected in the Flag-p54^{nrb} immunoprecipitation complexes and vice versa (Fig. 1D,E). Importantly, the co-IP was still detectable in the presence of RNase A (Fig. 1E). Colocalization of the endogenous p54^{nrb} and CARM1 further revealed that they colocalized in the nucleus in HeLa cells (Fig. 1F) and largely within paraspeckles, as revealed by *NEAT1* RNA in situ hybridization (ISH) and CARM1 immunostaining (Fig. 1G). Together, these results suggest that p54^{nrb} is a new substrate for CARM1 and that p54^{nrb} methylation by CARM1 may occur within paraspeckles.

*CARM1 deficiency leads to enhanced nuclear retention of mRNAs containing IR*Alus

We next asked whether p54^{nrb} methylation by CARM1 could alter paraspeckle-associated p54^{nrb} function. Since p54^{nrb} is involved in the nuclear retention of mRNAs containing IR*Alu*s in their 3′ UTRs (mRNA-IR*Alu*s) (Chen et al. 2008; Mao et al. 2011a), we first performed mRNA nuclear retention assays in the scramble and CARM1 knockdown cell lines with mRNA-IR*Alu*s reporter constructs as previously described (Chen et al. 2008). Constructs with a single *Alu* element or IR*Alu*s (originally from the 3′ UTR of the *Nicn1* gene) in the 3′ UTR of *egfp* mRNA were individually transfected into the scramble and CARM1 knockdown HeLa cells. Consistent with previous reports (Chen et al. 2008; Mao et al. 2011a), the expression of EGFP protein was repressed by IR*Alu*s, but not by a single *Alu*, in the 3′ UTR of *egfp* (Fig. 2A,B). This repressed EGFP expression was largely due to the nuclear retention of *egfp*-IR*Alu*s (Fig. 2A,B).

Strikingly, the EGFP fluorescence in CARM1 knockdown cells transfected with the EGFP-IR*Alu*s construct was much more significantly reduced than that in scramble cells (Fig. 2A). This enhanced repression effect was also confirmed by Western blotting with anti-GFP antibody (Fig. 2A, top right panels, lanes 2,4). Meanwhile, Northern blotting of transcripts of *egfp* from the same batch of transfected HeLa cells revealed that both transfections yielded comparable or higher levels of *egfp* mRNAs (Fig. 2A, bottom right panels, lanes 2,4), suggesting that the observed enhanced EGFP expression repression in CARM1 knockdown cells is post-transcriptional. We also observed similar phenomena using other constructs containing inserts of a single *Alu* element or IR*Alu*s derived from the 3′ UTR of the *Lin28* gene in the 3′ UTR of *egfp* mRNA (Supplemental Fig. S3A,B) and in other cell lines, such as in the scramble and CARM1 stable knockdown HEK293 cells (Supplemental Fig. S4A,B).

What mechanism accounts for reduced EGFP expression in CARM1 knockdown cells? Further analyses revealed that CARM1 knockdown strikingly enhanced the sequestration of mRNAs containing 3′ UTR IR*Alu*s in the nucleus. First, nuclear/cytoplasmic (N/C) RNA fractionation analyses in scramble and CARM1 knockdown cells individually transfected with *egfp-Alu* or *egfp*-IR*Alu*s constructs clearly showed that *egfp*-IR*Alu*s mRNA was more efficiently retained in the nuclei of CARM1 knockdown cells than those in the nuclei of scramble cells (Fig. 2B, left panels [lanes 3,4,7,8] and right panel), while the N/C ratio of *egfp-Alu* mRNA was not altered (Fig. 2B, left panels [lanes 1,2,5,6] and right panel). Second, visualization of the subcellular distribution of *egfp*-IR*Alu*s in scramble and CARM1 knockdown cells by RNA ISH at the single-cell level revealed that *egfp* mRNAs with IR*Alu*s were more highly enriched in the nucleus in CARM1 knockdown cells than those in scramble cells (Fig. 2C). Third, if CARM1 were essential for the paraspeckle-associated mRNA-IR*Alu*s nuclear retention, we would expect to observe that the endogenous mRNA-IR*Alu*s would have a different fate in CARM1 depletion cells. There are hundreds of mRNAs containing IR*Alu*s in their 3′ UTRs (Chen et al. 2008), and we chose a number of mRNAs that contain IR*Alu*s in their 3′ UTRs and are expressed well in HeLa and HEK293 cells (*nicn1*, *icmt*, *mrpl30*, and *pccb*) (Supplemental Fig. S5). For each of these mRNAs, CARM1 knockdown resulted in more efficient retention in the nucleus in both cell lines (Fig. 2D,E; Supplemental Figs. S4D, S6), while the N/C distribution of *actin* mRNA remained unchanged. For experiments shown in these figures, we used PCR probes that specifically recognize mRNAs with the extended 3′ UTRs that contain IR*Alu*s (Supplemental Fig. S5). Note that the longer isoform of each of the mRNAs containing IR*Alu*s examined increased its N/C ratio after knockdown of CARM1 (Fig. 2D; Supplemental Figs. S4D, S6A). We further used Northern blotting to confirm the subcellular distribution of two such endogenous mRNAs: *nicn1* (Fig. 2E) and *icmt* (Supplemental Fig. S6B). The long isoform of *nicn1* contains one pair of IR*Alu*s in its 3′ UTR, but the short isoform lacks IR*Alu*s. Correspondingly, the *nicn1* long isoform is preferentially localized to the nucleus, while the short one is almost exclusively cytoplasmic (Fig. 2E; Chen et al. 2008). Importantly, knockdown of CARM1 increased the amount of *nicn1* long isoform retained in the nucleus (Fig. 2E), while the subcellular distribution of the *nicn1* short isoform and *actin* mRNA remained unaltered (Fig. 2E). Such altered nuclear retention regulation by CARM1 was also seen in another examined endogenous mRNA, *icmt* (Supplemental Fig. S6B), by Northern blotting. Together, these results demonstrate that the absence of CARM1 leads to an enhanced nuclear retention of mRNAs containing 3′ UTR IR*Alu*s.

Recently, *NEAT1* was shown to bind to hundreds of active chromatin sites in MCF7 cells (West et al. 2014). We found that ~40% of such genes contain at least one pair of IR*Alu*s in their 3′ UTRs expressed in MCF7 cells (Fig. 2F), implying that these transcribed nascent RNAs and corresponding mRNAs with 3′ UTR IR*Alu*s are located close to paraspeckles and thus are capable of association with paraspeckle protein p54^{nrb} for their nuclear retention.

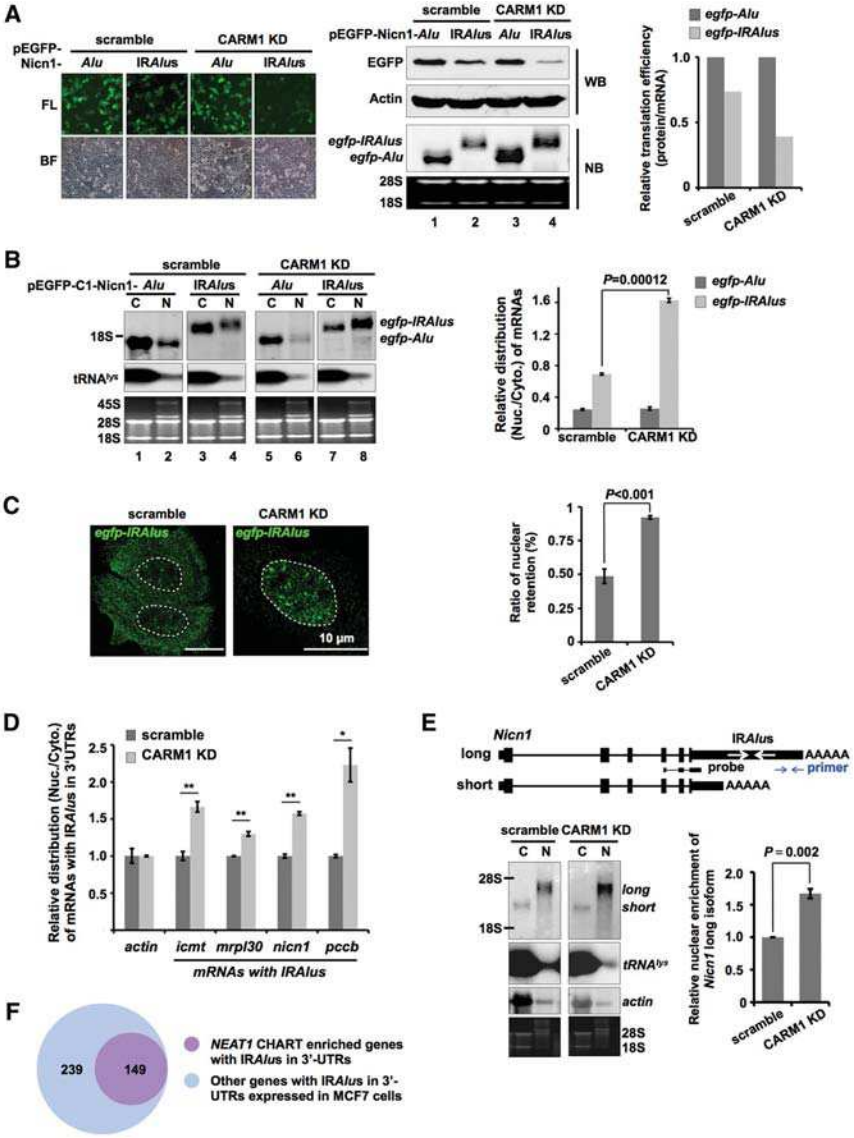

Figure 2. CARM1 deficiency enhances nuclear retention of mRNAs containing IR*Alu*s. (*A*) CARM1 knockdown (KD) suppresses EGFP expression of *egfp* mRNA containing IR*Alu*s in its 3′ UTR. (*Left*) IR*Alu*s and *Alu* from the 3′ UTR of *Nicn1* were inserted into the 3′ UTR of *egfp* mRNA (Chen et al. 2008). Stable HeLa cell lines with the scramble shRNA treatment and CARM1 knockdown were transfected with the indicated plasmids, and fluorescence was observed 24 h after transfection. (FL) Fluorescence; (BF) bright field. (*Middle*) The expression of EGFP and transcripts of *egfp* from the same batch of transfected HeLa cells as described in the *left* panels was investigated by Western blotting by probing with anti-EGFP antibody and by Northern blotting by probing with a Dig-labeled *egfp* fragment. Actin was used as loading control for Western blotting. Equivalent amounts of total RNAs were loaded for Northern blotting as indicated by 28S and 18S rRNAs. (*Right*) The relative translation efficiency (the relative intensity of each corresponding band from Western blotting and Northern blotting shown in the *middle* panels) of *egfp-Alu* mRNA and mRNA with *egfp*-IR*Alu*s in scramble and CARM1 knockdown cells. (*B*) CARM1 deficiency significantly enhances the nuclear retention of *egfp* mRNA with IR*Alu*s. (*Left*) Cytoplasmic and nuclear RNAs were isolated from the same batch of transfected HeLa cells used in *A* and then resolved on a denaturing agarose gel. Transcripts of *egfp*-tagged RNAs were probed with a Dig-labeled *egfp* fragment. $tRNA^{lys}$ and 45S rRNA were used as markers for cytoplasmic/nuclear RNA isolation. Equivalent amounts of RNAs from different subcellular compartments were loaded as indicated by 28S and 18S rRNAs. (*Right*) The relative subcellular distribution of RNAs with IR*Alu*s or single *Alu*-containing RNAs was quantified from the *left* panels by ImageJ and normalized to the relative amount of $tRNA^{lys}$. The ratio was obtained by comparing the value of each nuclear-retained fractionation with those of the cytoplasmic distributed RNAs. (*C*) Enhanced *egfp* mRNAs with IR*Alu*s are retained in the nucleus upon CARM1 deficiency, as revealed by RNA ISH. (*Left*) The *egfp* mRNAs with IR*Alu*s were probed with a Dig-labeled antisense *egfp* probe in HeLa cells transfected with the indicated plasmids, and representative images are shown. The white dotted line indicates the nucleus. (*Right*) Statistical analysis of the *left* panel. More than 300 transfected cells were analyzed after each transfection, and the *P*-value from a one-tailed *t*-test in the pairwise comparison is shown. (*D*) CARM1 knockdown enhances the nuclear retention of other endogenous mRNAs with IR*Alu*s. RT-qPCR analyzed a number of other endogenous mRNAs with IR*Alu*s using nuclear and cytoplasmic fractionated RNAs. Primers to detect RNAs with IR*Alu*s were designed downstream from IR*Alu*s in 3′ UTRs (Supplemental Fig. S5). The relative subcellular distribution of each RNA with IR*Alu*s was normalized to the relative amount of *actin* mRNA. (*E*) CARM1 knockdown promotes the nuclear retention of endogenous *nicn1* mRNA in HEK293 cells. (*Top*) A schematic drawing of transcripts of the *Nicn1* gene containing two isoforms (Chen et al. 2008). (*Bottom left*) Note that the long isoform contains a pair of IR*Alu*s in its 3′ UTR and is preferentially retained in the nucleus. Cytoplasmic and nuclear RNA fractionation of scramble and CARM1 knockdown cells followed by Northern blotting to detect *nicn1* mRNAs. $tRNA^{lys}$ and *actin* revealed a successful cytoplasmic and nuclear fractionation. Equivalent amounts of RNA from different compartments were loaded as indicated by 28S and 18S rRNAs. (*Bottom right*) The relative subcellular distribution of the long isoform of *nicn1* mRNA was quantified from the *left* panels by ImageJ and normalized to the relative amount of nuclear *actin* mRNA from the same stripped membrane. (*F*) Genes containing IR*Alu*s in 3′ UTRs are enriched in the *NEAT1*-bound active chromatin sites. *NEAT1* CHART-seq data in MCF7 cells were retrieved from West et al. (2014). Genes containing IR*Alu*s in 3′ UTRs were identified from RefSeq by a home-brewed pipeline. In *B*, *D*, and *E*, error bars represent ±SD in triplicate experiments. (*) $P < 0.05$; (**) $P < 0.01$; $n = 3$.

*p54^{nrb} methylation by CARM1 regulates nuclear retention of mRNAs containing IR*Alus

The next question is whether this CARM1-regulated nuclear retention is dependent on p54^{nrb}. To answer this question, we knocked down CARM1 or p54^{nrb} and then followed the expression and the subcellular distribution of the IR*Alu*s-containing reporter plasmid Flag-mcherry-IR*Alu*s. The pair of IR*Alu*s used in this construct is from the 3′ UTR of the *Nicn1* gene (Chen et al. 2008). While knockdown of CARM1 reduced Flag-mcherry expression (Fig. 3A, lane 2; Supplemental Fig. S7A) with an enhanced nuclear retention of *Flag-mcherry-IRAlu*s mRNAs (Fig. 3B), as other assays revealed (Fig. 2; Supplemental Figs. S3, S4), knockdown of p54^{nrb} enhanced Flag-mcherry expression (Fig. 3A, lane 4; Supplemental Fig. S7A) with a reduced nuclear retention of *Flag-mcherry-IRAlu*s mRNAs (Fig. 3B). Double knockdown of CARM1 and p54^{nrb} showed little change in both protein expression and mRNA nuclear retention (Fig. 3A [lane 3], B). These results confirm that the nuclear retention of mRNAs with 3′ UTR IR*Alu*s is mediated by the paraspeckle-localized protein p54^{nrb} and that CARM1 suppresses this nuclear retention pathway (Supplemental Fig. S7C).

We next asked whether the catalytic activity of CARM1 is required for the observed nuclear retention. We expressed the wild-type or the catalytically inactive E266Q mutant of CARM1 (Lee et al. 2002) in scramble or

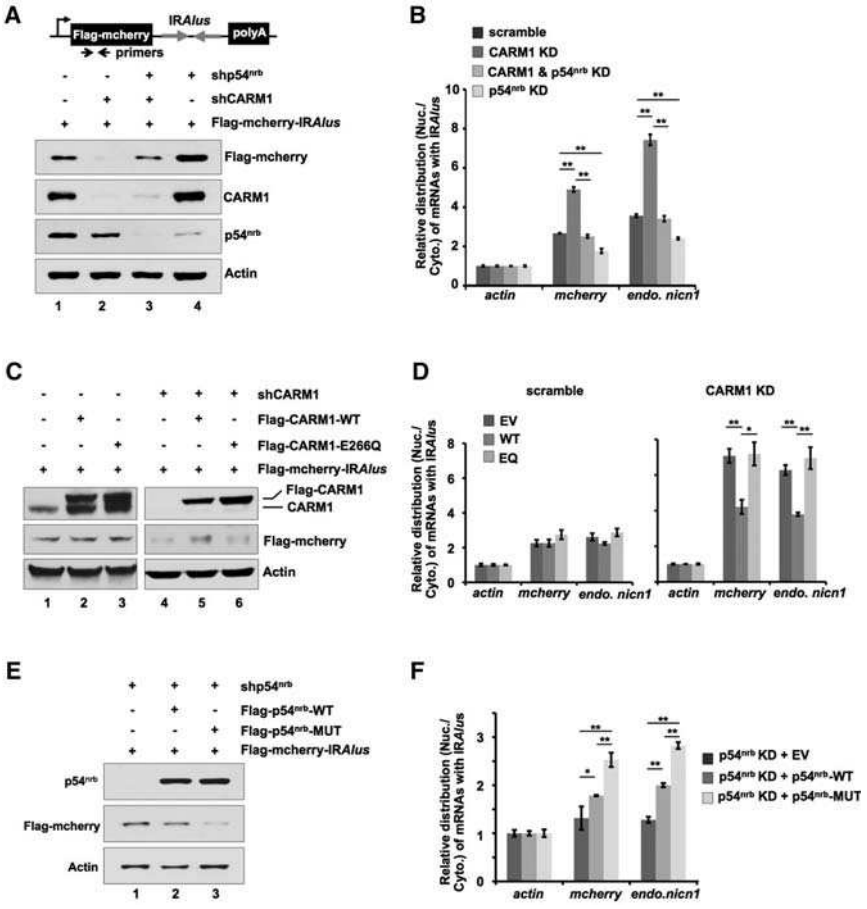

Figure 3. IR*Alu*s mRNA nuclear retention is achieved through p54^{nrb} and requires the catalytic activity of CARM1. (*A*) IR*Alu*s mRNAs nuclear retention is achieved through p54^{nrb}. (*Top*) A schematic drawing of Flag-mcherry-containing IR*Alu*s in its 3′ UTR (Flag-mcherry-IR*Alu*s). (*Bottom*) Knockdown of CARM1 (lane *2*) or p54^{nrb} (lane *4*) or double knockdown of CARM1 and p54^{nrb} (lane *3*) in HeLa cells expressing Flag-mcherry-IR*Alu*s, followed by Western blotting. Note that knockdown of CARM1 suppresses Flag-mcherry expression, while knockdown of p54^{nrb} increases Flag-mcherry expression. (*B*) The altered Flag-mcherry protein expression in *A* corresponds to altered nuclear retention of transcripts of *Flag-mcherry-IRAlu*s. The relative subcellular distribution of transcripts of *Flag-mcherry-IRAlu*s from the same batch of transfected cells as described in *A* was investigated by RT-qPCR by probing *mcherry*. The level of nuclear retention was presented as the ratio of nuclear-retained transcripts of *Flag-mcherry-IRAlu*s to those in the cytoplasm after normalization to the relative amount of *actin* mRNA in each fraction. The endogenous mRNA with 3′ UTR IR*Alu*s was also assayed and normalized in the same way. (*C*) IR*Alu*s mRNA nuclear retention is dependent on the catalytic activity of CARM1. Reintroduction of wild-type (WT) CARM1 or the catalytic inert E266Q-CARM1 into scramble (lanes *2*,*3*) or CARM1 knockdown (KD) (lanes *5*,*6*) HeLa cells expressing Flag-mcherry-IR*Alu*s, followed by Western blotting. Note that expression of wild-type CARM1 but not the E266Q-CARM1 in CARM1 knockdown cells could rescue the suppressed expression of Flag-mcherry-IR*Alu*s. (*D*) Altered Flag-mcherry protein expression in *C* corresponds to the altered nuclear retention of transcripts of *Flag-mcherry-IRAlu*s. The relative subcellular distribution of transcripts of *Flag-mcherry-IRAlu*s and the endogenous mRNA with 3′ UTR IR*Alu*s from the same batch of transfected cells as described in *C* were investigated by RT-qPCR. See *B* for details. (*E*) Mutation of CARM1 methylation sites on p54^{nrb} enhances the p54^{nrb} -mediated mRNA nuclear retention. Reintroduction of the lysine replacement of Arg357, Arg365, and Arg378 (R357K, R365K, and R378K) of p54^{nrb} (p54^{nrb}-MUT; lane *3*) into p54^{nrb} knockdown cells resulted in an enhanced mCherry suppression compared with that of wild-type p54^{nrb} (lane *2*), as revealed by Western blotting. (*F*) Altered Flag-mcherry expression in *E* corresponds to the altered nuclear retention of transcripts of *Flag-mcherry-IRAlu*s. The relative subcellular distribution of transcripts of *Flag-mcherry-IRAlu*s and the endogenous mRNA with 3′ UTR IR*Alu*s from the same batch of transfected cells as described in *E* were investigated by RT-qPCR. See for details. In *B*, *D*, and *F*, error bars represent ±SD in triplicate experiments. (*) $P < 0.05$; (**) $P < 0.01$; $n \geq 3$.

CARM1 stable knockdown cell lines followed by the reporter assays described above (Fig. 3A,B). We found that reintroduction of the wild-type CARM1, but not the E266Q-CARM1, into CARM1 knockdown cells in which p54^{nrb} is largely unmethylated due to CARM1 knockdown could largely restore the reduced Flag-mcherry expression (Fig. 3C, lanes 4–6; Supplemental Fig. S7B), the enhanced nuclear retention of *Flag-mcherry-IRAlu*s mRNAs, and the endogenous mRNA with 3′ UTR IR*Alu*s (Fig. 3D). However, reintroduction of either wild-type or E266Q-CARM1 into scramble treated cells in which CARM1 exists and p54^{nrb} is methylated had little effect on the reporter assay or the endogenous mRNA with 3′ UTR IR*Alu*s (Fig. 3C [lanes 1–3], D).

Moreover, we set up to examine whether the p54^{nrb} variant carrying the lysine replacement of Arg357, Arg365, and Arg378 (R357K, 365K, and R378K) that showed a reduced p54^{nrb} methylation by CARM1 (Fig. 1C) could enhance the p54^{nrb}-mediated mRNA nuclear retention. Reintroduction of the p54^{nrb} variant that carries these three point mutants (R357K, 365K, and R378K) into p54^{nrb} knockdown cells not only was able to restore the p54^{nrb} function but also exhibited a stronger effect on protein expression suppression and the corresponding mRNA nuclear retention in the reporter assay (Fig. 3E,F). Meanwhile, a similar observation was also seen in the examined endogenous mRNA with 3′ UTR IR*Alu*s (Fig. 3F). Together, these results strongly suggest that CARM1 methylation on p54^{nrb} attenuates the p54^{nrb}-mediated mRNA nuclear retention.

*The absence of CARM1 enhances the association of p54^{nrb} and mRNAs with IR*Alus

How does p54^{nrb} methylation by CARM1 alter mRNA nuclear retention? Since p54^{nrb} can bind to IR*Alu*s mRNAs and subsequently retain them in the nucleus (Prasanth et al. 2005; Chen et al. 2008; Mao et al. 2011a), we performed p54^{nrb} RNA immunoprecipitation (RIP) assays to examine whether the methylation of p54^{nrb} could alter its binding activity with the IR*Alu*s mRNAs. Both formaldehyde cross-linking RIP and UV cross-linking RIP with the anti-p54^{nrb} antibody in scramble and CARM1 knockdown cell lines revealed that the absence of CARM1 augmented the association of p54^{nrb} and mRNAs with IR*Alu*s (Fig. 4A,B). Importantly, the lysine replacement of Arg357, Arg365, and Arg378 (R357K, 365K, and R378K) of Flag-p54^{nrb} that showed a reduced p54^{nrb} methylation by CARM1 (Fig. 1C) also increased its ability to bind to mRNAs with IR*Alu*s compared with the wild-type Flag-p54^{nrb} (Fig. 4C), with an anti-Flag antibody UV cross-linking RIP in HeLa cells.

To further confirm that p54^{nrb} unmethylated in its coiled-coil domain has an increased ability to bind to mRNA-IR*Alu*s, we then performed a reciprocal pull-down assay by tagging an aptamer tRSA (Iioka et al. 2011) to IR*Alu*s RNA (tRSA-IR*Alu*s) (Fig. 4D). Following tRSA immunoprecipitation with nuclear extracts, we found that tRSA-IR*Alu*s, but not the tRSA alone, was preferentially associated with p54^{nrb} (Fig. 4D). Overexpression of CARM1 resulted in reduced binding of tRSA-IR*Alu*s with p54^{nrb} (Fig. 4D), confirming that methylation by CARM1 on p54^{nrb} reduced its ability to bind to RNA-IR*Alu*s. Moreover, the partially purified Flag-p54^{nrb}-MUT carrying the lysine replacements of R357K, 365K, and R378K significantly increased its ability to bind to the in vitro transcribed IR*Alu*s compared with the wild-type protein (Fig. 4E). Since R357 and R365 are located at the coiled-coil domain and R378 is located very close to this domain at the C terminus of p54^{nrb} (Supplemental Fig. S2D), these results strongly suggest that methylation on p54^{nrb} at or near the coiled-coil domain by CARM1 reduces its capability to associate with RNAs containing IR*Alu*s.

p54^{nrb} methylation at or near the coiled-coil domain by CARM1 alters its binding to dsRNAs

How does unmethylated p54^{nrb} bind to mRNAs with IR*Alu*s? Since p54^{nrb} is known to bind to inosine-containing RNAs (Zhang and Carmichael 2001), one possibility is that p54^{nrb} binds to edited mRNA-IR*Alu*s (Prasanth et al. 2005; Chen et al. 2008). However, some extensively adenosine (A)-to-inosine (I) edited mRNA-IR*Alu*s were also exported to the cytoplasm (Prasanth et al. 2005; Chen et al. 2008; Hundley et al. 2008; Elbarbary et al. 2013), and knockdown of ADAR1 did not alter the nuclear retention of these RNAs (Elbarbary et al. 2013), indicating that p54^{nrb} can bind to RNAs by recognizing other RNA structures, such as dsRNAs formed by the IR*Alu*s at the 3′ UTR of mRNAs. We therefore examined whether p54^{nrb} could bind to dsRNAs and whether p54^{nrb} methylation by CARM1 could selectively alter its binding to these molecules.

The in vitro binding assays revealed that full-length of p54^{nrb} bound to both dsRNAs and ssRNAs (Fig. 5A); importantly, knockdown of CARM1 altered the binding ability of p54^{nrb} to only dsRNAs but not to ssRNAs (Fig. 5A). With a newly developed antibody (620me) that specifically recognizes the methylated R357 and R365 on a p54^{nrb} peptide (Fig. 5B, left panels), we found that the methylated p54^{nrb} (620me) was enriched in ssRNA but was barely detected in dsRNA pull-downs (Fig. 5B, right panels). This observation further suggests that CARM1 methylation on p54^{nrb} reduces its binding capacity to dsRNAs. Moreover, the partially purified Flag-p54^{nrb}-MUT carrying the lysine replacements of R357K, 365K, and R378K promoted its binding capability to the in vitro transcribed dsRNAs but showed little binding alteration to ssRNAs (Fig. 5C). These results thus support the notion that p54^{nrb} methylation by CARM1 alters its binding to dsRNAs and that the unmethylated p54^{nrb} binds more strongly to dsRNAs.

As it has been reported that p54^{nrb} bound to ssDNAs (and RNAs) through its N terminus and to DNA through its C terminus (Yang et al. 1993), we speculated that the coiled-coil domain at the C terminus of p54^{nrb} might mediate its binding to dsRNAs, such as mRNAs

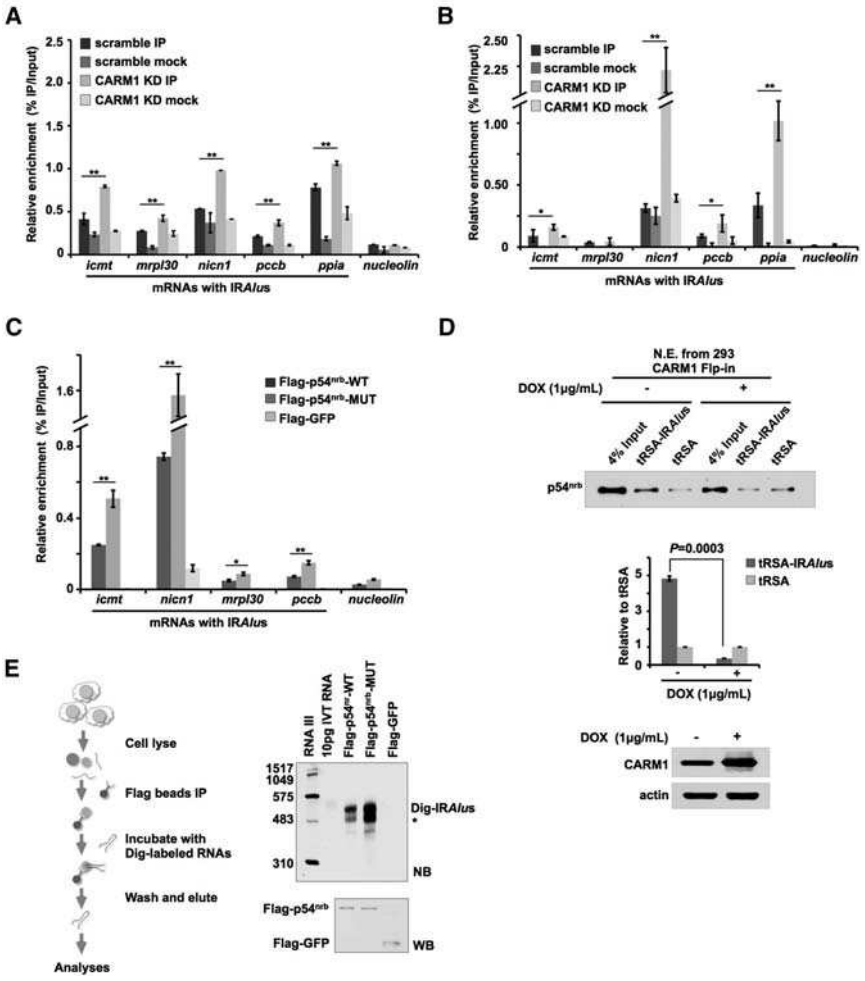

Figure 4. p54^{nrb} methylation reduces its ability to bind to IR*Alu*s mRNAs. (*A*) CARM1 deficiency increases the association of p54^{nrb} and the endogenous IR*Alu*s mRNAs. The association between p54^{nrb} and mRNAs with IR*Alu*s was assayed by formaldehyde cross-linking RIP from scramble or CARM1 knockdown HeLa cells using anti-p54^{nrb} and anti-IgG followed by RT-qPCR. Bar plots represent the fold enrichments of RNAs immunoprecipitated by anti-p54^{nrb} or anti-IgG over the same amount of input across different samples, and error bars represent SD in triplicate experiments. *Nucleolin* mRNA was a control that does not bind to p54^{nrb}. (*B*) CARM1 deficiency increases the association of p54^{nrb} and endogenous IR*Alu*s mRNAs, as assayed by UV cross-linking RIP from scramble or CARM1 knockdown HeLa cells using anti-p54^{nrb} and anti-IgG followed by RT-qPCR. See *A* for details. (*C*) Lysine replacement of Arg357, Arg365, and Arg378 (R357K, R365K, and R378K) of p54^{nrb} (p54^{nrb}-MUT) increases the association of p54^{nrb} and endogenous IR*Alu*s mRNAs. The interaction of p54^{nrb} and endogenous IR*Alu*s mRNAs was assayed by RIP in HeLa cells expressing Flag-p54^{nrb}, Flag-p54^{nrb}-MUT, or Flag-EGFP followed by RT-qPCR. See *A* for details. (*D*) CARM1 overexpression attenuates the interaction between p54^{nrb} and IR*Alu*s RNA. (*Top*) tRSA-RNA pull-downs (Iioka et al. 2011) using in vitro transcribed tRSA-tagged IR*Alu*s RNAs were performed in nuclear extracts of 293 CARM1 Flp-in cells with or without 1 μg/mL doxycycline (DOX) induction. (*Middle*) The quantitative analyses of the *top* panel from three independent experiments. (*Bottom*) CARM1 expression was induced upon the DOX treatment, as revealed by Western blotting. (*E*) Partially purified triple mutations of R357K, R365K, and R378K of p54^{nrb} (p54^{nrb}-MUT) exhibit increased ability to bind to IR*Alu*s RNAs. (*Left*) A schematic drawing of the experimental flow. (*Right*) Flag-p54^{nrb}-wt, but not Flag-EGFP, exhibited an ability to bind to Dig-labeled IR*Alu*s RNA; Flag-p54^{nrb}-MUT showed an enhanced ability to bind to IR*Alu*s RNA.

containing IR*Alu*s. This is indeed the case. Incubation of ssRNAs or dsRNAs with different Flag-tagged p54^{nrb} truncations individually expressed in HeLa cells revealed that the truncation of p54^{nrb} containing two RRM domains preferred to bind to ssRNAs, and the truncation of p54^{nrb} with the addition of the coiled-coil domain exhibited a much higher capacity to bind to dsRNAs (Fig. 5D,E). Importantly, while the partially purified Flag-tagged p54^{nrb} carrying only RRM domains showed little association to the in vitro transcribed IR*Alu*s, the inclusion of the coiled-coiled domain to this truncation significantly increased its ability to bind to IR*Alu*s (Fig. 5F), confirming that the coiled-coil domain of p54^{nrb} mediates its binding to dsRNAs, including mRNA-IR*Alu*s. Together, these results strongly suggest that p54^{nrb} methylation by CARM1 at or near the coiled-coil domain alters the interaction between dsRNAs and p54^{nrb} via the coiled-coil domain.

CARM1 inhibits NEAT1 *transcription and reduces paraspeckle formation*

We showed that CARM1 methylated the coiled-coil domain of p54^{nrb}, resulting in the reduced binding of p54^{nrb} to mRNAs containing IR*Alu*s. CARM1 is also known for its activity in transcription regulation (Chen et al. 1999). CARM1 largely functions as a transcriptional coactivator (Chen et al. 1999) but also acts as a transcriptional cosuppressor (Xu et al. 2001). We then asked whether the paraspeckle-localized CARM1 could also affect *NEAT1* transcription.

Surprisingly, we found that in CARM1 knockdown stable cell lines, the expression of both isoforms of *NEAT1* was increased (Fig. 6A). Correspondingly, the number of paraspeckles was also modestly increased in both CARM1 stable knockdown HeLa cells (Fig. 6B) and HEK293 cells (Fig. 6C). CARM1 chromatin

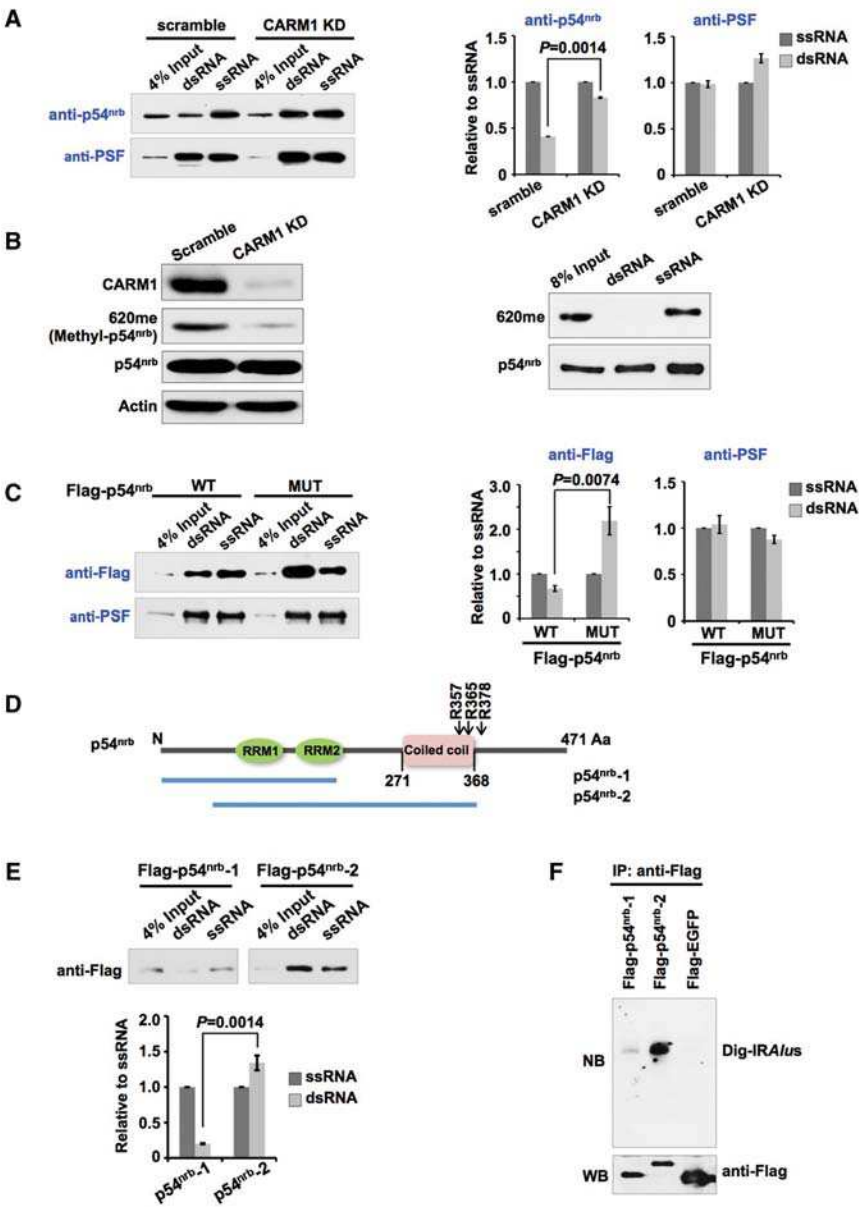

Figure 5. p54^{nrb} methylation by CARM1 alters its binding to dsRNAs. (*A*) CARM1 knockdown affects p54^{nrb} binding to dsRNAs but has little effect on ssRNAs. Biotin-labeled dsRNAs (double-stranded-*egfp* 76–495) or ssRNAs (single-stranded-*egfp* 1–798) were made from in vitro transcription (IVT). Nuclear extracts of scramble or CARM1 knockdown (KD) HeLa cells were incubated with biotin-dsRNA or biotin-ssRNA followed by anti-biotin pull-down and Western blotting with antibodies for anti-p54^{nrb} and anti-PSF. (*Right*) The quantitative analyses of the *left* panels from three independent experiments. (*B*) Methylated p54^{nrb} binds to few dsRNAs. (*Left*) The 620me antibody was developed to specifically recognize the methylated p54^{nrb}. Western blotting analyzed the specificity of 620me antibody purified from rabbit serum immunized with methylated peptides of R357 and R365. p54^{nrb} and Actin antibodies were used as controls. (*Right*) The methylated p54^{nrb} (620me) was enriched by biotin-ssRNA but not by biotin-dsRNA pull-downs from wild-type HeLa cell nuclear extracts. See *A* for details. (*C*) Lysine replacement of Arg357, Arg365, and Arg378 (R357K, 365K, and R378K) of p54^{nrb} (p54^{nrb}-MUT) increases the association of p54^{nrb} and dsRNAs. (*Right*) The quantitative analyses of the *left* panels from three independent experiments. See *A* for details. (*D*) A schematic drawing of different truncations of p54^{nrb} used in *E* and *F*. (*E*) A different domain of p54^{nrb} selectively binds to ssRNAs or dsRNAs. (*Top*) Nuclear extracts of HeLa cells transfected with different p54^{nrb} truncations were incubated with biotin-dsRNAs or biotin-ssRNAs followed by anti-biotin pull-down and Western blotting with anti-Flag. (*Bottom*) The quantitative analyses of the *top* panels from three independent experiments. (*F*) Partially purified truncation of p54^{nrb} selectively binds to IR*Alu*s RNAs. Different p54^{nrb} truncations shown in *D* were purified and incubated with Dig-labeled IR*Alu*s RNAs. See Figure 4E for details. In *A*, *C*, and *E*, error bars represent ±SD in triplicate experiments. *P*-values from one-tailed *t*-test in the pairwise comparison are shown.

immunoprecipitation (ChIP) revealed that CARM1 was enriched at the promoter of the *NEAT1* gene (Fig. 6D). Further studies by nuclear run-on (NRO) assays showed that the transcription of nascent transcripts of *NEAT1* was increased upon CARM1 knockdown, confirming the notion that CARM1 could regulate *NEAT1* transcription as a transcriptional cosuppressor.

Collectively, we propose a model for CARM1-regulated nuclear retention of mRNAs containing IR*Alu*s at paraspeckles. p54^{nrb} methylation by CARM1 at the coiled-coil domain reduces its ability to bind to mRNAs containing IR*Alu*s (Figs. 2–5). This is in coordination with the transcriptional suppression of CARM1 at the *NEAT1* promoter (Fig. 6). Thus, CARM1 can synergistically act at two levels within paraspeckles to regulate its function for mRNA nuclear retention (Fig. 7I).

CARM1 is involved in the poly(I:C)-stimulated enhancement of nuclear retention regulation

Finally, it will be of interest to identify conditions that affect CARM1-regulated mRNA nuclear retention within paraspeckles. It is known that the transcription of *NEAT1* RNAs and the formation of paraspekles are induced upon virus infection or poly(I:C) treatment (Saha et al. 2006; Zhang et al. 2013a; Imamura et al. 2014). We therefore

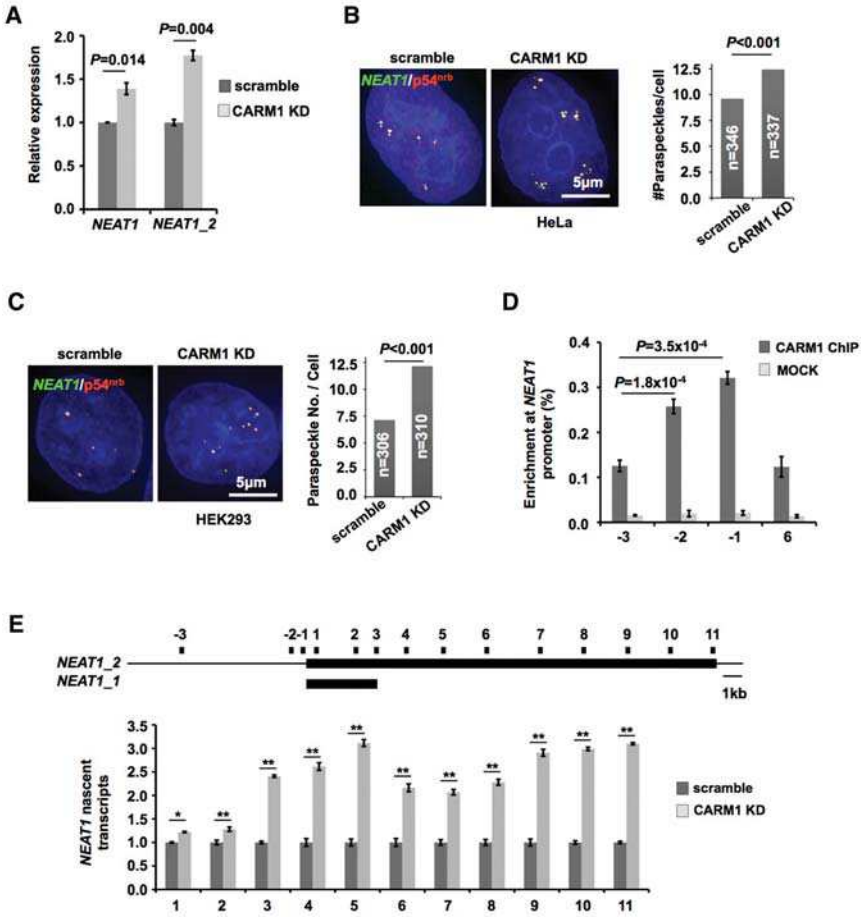

Figure 6. CARM1 is enriched at the *NEAT1* promoter and inhibits *NEAT1* transcription and paraspeckle formation. (*A*) CARM1 deficiency promotes the expression of both isoforms of *NEAT1*. (*B*) CARM1 knockdown increases paraspeckle formation. (*Left*) Colocalization of *NEAT1* RNA (green) and p54^{nrb} protein (red) revealed paraspeckles in scramble and CARM1 knockdown (KD) HeLa cells. (*Right*) Statistical analysis of numbers of paraspeckles from >300 cells in scramble and CARM1 knockdown HeLa cells. The *P*-value from a one-tailed *t*-test in the pairwise comparison is shown. (*C*) CARM1 knockdown increases paraspeckle formation in HEK293 cells. (*D*) CARM1 is enriched on the promoter region of *NEAT1*. CARM1 ChIP followed by qPCR analyzed the occupation of CARM1 on the *NEAT1* gene. The positions of examined primers are shown in *E*. (*E*) CARM1 deficiency promotes the transcription of nascent *NEAT1*. (*Top*) A schematic drawing indicates the primer sets used. (*Bottom*) A crude preparation of nuclei was subjected to NRO assays under the indicated conditions in HeLa cells. Nascent transcription of *NEAT1* detected from scramble nuclei was defined as one. In *A*, *D*, and *E*, error bars represent ±SD in triplicate experiments. (*) $P < 0.05$; (**) $P < 0.01$; $n \geq 3$.

investigated whether CARM1-regulated nuclear retention is affected by poly(I:C) treatment. In our experiments, transfection of poly(I:C) led to increased expression of *interferon β* and *NEAT1* RNAs (Fig. 7A,B). Importantly, we found that the enrichment of CARM1 at the *NEAT1* promoter was reduced upon poly(I:C) treatment (Fig. 7C), corresponding to the observed up-regulation of *NEAT1* RNAs (Fig. 7B). Furthermore, the expression of *NEAT1* RNAs remained at high levels in CARM1 knockdown cells, and *NEAT1* expression could not be further induced upon poly(I:C) treatment (Fig. 7D). In addition, we found that the treatment of cells with poly(I:C) led to a strong reduction of p54^{nrb} methylation on these arginine residues (Fig. 7E), while the expression of p54^{nrb} remained unchanged. Finally, poly(I:C) treatment also resulted in an enhanced nuclear retention of a number of examined mRNAs containing IR*Alu*s (Fig. 7F). Interestingly, we found that upon poly(I:C) treatment, the expression of CARM1 protein remained largely unchanged (Fig. 7G), while the paraspeckle-localized CARM1 was significantly reduced (Fig. 7H), indicating that CARM1 may rapidly change its subcellular localization with an unknown mechanism upon the stress treatment. Taken together, these results suggest that actions of CARM1 at p54^{nrb} methylation and *NEAT1* transcription synergistically work together to regulate the export of transcripts containing IR*Alu*s from paraspeckles under certain cellular stresses, such as the poly(I:C) treatment (Fig. 7I).

Discussion

Paraspeckles play a role in gene regulation through nuclear retention mediated by the association of their key protein component, p54^{nrb}, with mRNAs containing inverted repeats (*Alu* repeats in humans) in their 3′ UTRs (Prasanth et al. 2005; Chen et al. 2008; Chen and Carmichael 2009; Mao et al. 2011a). Such nuclear-retained mRNAs are inefficiently exported to the cytoplasm, resulting in silencing of gene expression. However, the level of nuclear retention of transcripts containing IR*Alu*s is variable, with some such mRNAs located in the nucleus, while others are in the cytoplasm (Prasanth et al. 2005; Chen et al. 2008; Hundley et al. 2008; Chen and Carmichael 2009; Elbarbary et al. 2013). How the nuclear retention of mRNAs containing IR*Alu*s at paraspeckles is regulated has remained elusive. Here we demonstrate that CARM1 is a novel component of paraspeckles (Fig. 1). Disruption of CARM1 significantly enhances the nuclear retention of mRNAs containing 3′ UTR IR*Alu*s and represses gene expression (Fig. 2; Supplemental Figs. S3, S4, S6).

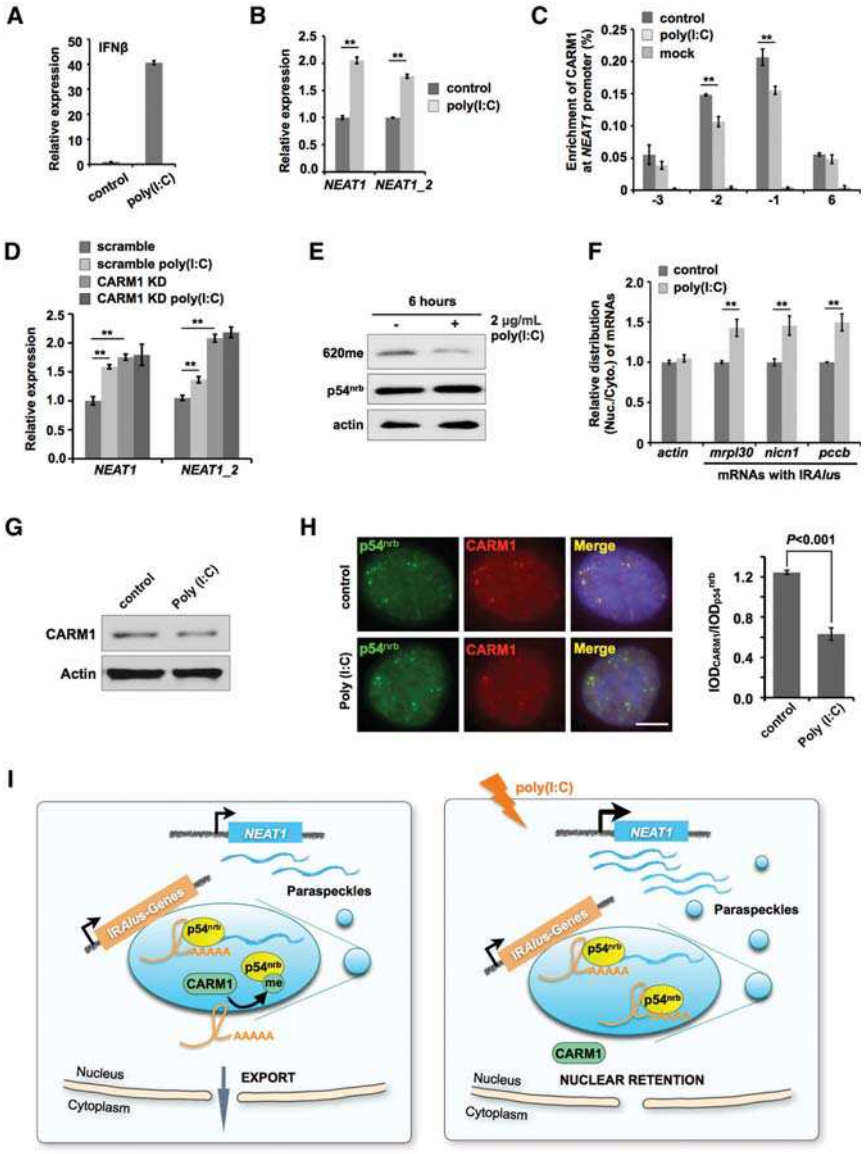

Figure 7. CARM1 is involved in the poly(I:C)-stimulated enhancement of nuclear retention. (*A*) Poly(I:C) treatment induces the expression of IFNβ. HeLa cells were transfected with 2 μg/mL poly(I:C) for 6 h and then harvested for analysis. (*B*) Poly(I:C) treatment induces *NEAT1* expression. (*C*) Poly(I:C) treatment reduces the occupancy of CARM1 at the *NEAT1* promoter. HeLa cells were transfected with poly(I:C) for 6 h and then harvested for CARM1 ChIP followed by qPCR. Data are presented as the percentage of CARM1 coprecipitating DNAs along the *NEAT1* gene versus input under each indicated condition. (*D*) Poly(I:C) treatment induces *NEAT1* expression in scramble-treated HeLa cells but not in CARM1 knockdown (KD) HeLa cells. (*E*) Poly(I:C) treatment reduces $p54^{nrb}$ methylation. HeLa cells were transfected with 2 μg/mL poly(I:C) for 6 h and then harvested for Western blotting analyses. (*F*) Poly(I:C) treatment enhances the nuclear retention of mRNAs containing IR*Alu*s. HeLa cells were transfected with poly(I:C) for 6 h and then harvested for the nuclear and cytoplasmic fractionations. The relative subcellular distribution of transcripts of endogenous transcripts with IR*Alu*s was investigated by RT-qPCR, normalized to the relative amount of *actin* mRNA in each fractionation, and compared with control HeLa cells. (*G*) The expression of CARM1 remains unchanged upon poly(I:C) treatment, as revealed by Western blotting. (*H*) The poly(I:C) treatment attenuates CARM1 localization to paraspeckles. (*Left*) Control and poly(I:C) transfected HeLa cells were stained with anti-$p54^{nrb}$ and anti-CARM1 antibodies, and representative images are shown. (*Right*) The statistics of $p54^{nrb}$ and CARM1 colocalization. The IODs (integrated optical densities) of punctuated anti-CARM1 and anti-$p54^{nrb}$ signals were measured by Image-Pro Plus from images taken with the same parameters ($n > 100$ double-positive staining cells). The ratio of IOD_{CARM1} to $IOD_{p54}{}^{nrb}$ was used to evaluate the extent of colocalization. The *P*-value from a one-tailed *t*-test in the pairwise comparison is shown. (*I*) A model of how the nuclear retention of IR*Alu*s mRNAs at paraspeckles is regulated. (*Left*) Under normal conditions, CARM1 suppresses *NEAT1* transcription and paraspeckle formation and also methylates $p54^{nrb}$, resulting in the reduced ability to bind to mRNAs containing IR*Alu*s. (*Right*) Upon appropriate stimulation, such as upon poly(I:C) treatment, actions of CARM1 are attenuated, resulting in an increased expression of *NEAT1* RNA, unmethylated $p54^{nrb}$, and enhanced nuclear retention of IR*Alu*s mRNAs at paraspeckles. See the text for details. In *B–D* and *F*, error bars represent ±SD in triplicate experiments. (**) $P < 0.01$; $n = 3$.

To achieve this regulation, CARM1 methylates $p54^{nrb}$ (Fig. 1; Supplemental Figs. S1, S2) and reduces its ability to associate with dsRNAs, such as mRNAs with IR*Alu*s (Figs. 4, 5). On the other hand, CARM1 suppresses *NEAT1* transcription and inhibits paraspeckle formation (Fig. 6).

While $p54^{nrb}$ is required for nuclear retention of mRNAs with 3′ UTR IR*Alu*s, the catalytic activity of CARM1 is also required for this effect (Fig. 3). How is binding of $p54^{nrb}$ to mRNA-IR*Alu*s achieved? Since it is known that $p54^{nrb}$ binds to inosine-containing RNAs (Zhang and Carmichael 2001) and that a strong correlation between A-to-I RNA editing and retention was seen in mRNAs containing inverted repeats (Prasanth et al. 2005; Chen and Carmichael 2008; Chen et al. 2008), it has been thought that one of the consequences of *Alu* RNA editing is to retain edited mRNAs within nuclear paraspeckles. However, some mRNAs with edited IR*Alu*s in their 3′ UTRs were also observed in the cytoplasm (Chen et al. 2008; Hundley et al. 2008). Knockdown of ADAR1, which is responsible for A-to-I RNA editing, has little effect on the export of nuclear-retained IR*Alu*s

mRNAs (Elbarbary et al. 2013). These results thus suggested that another nuclear retention signal is required for p54^{nrb}-mediated mRNA nuclear retention in addition to RNA editing. Another formal possibility is that long imperfect duplexes formed by IR*Alu*s in the 3′ UTRs of genes might influence gene regulation even in the absence of editing. We showed that such unique hairpin structures can directly bind to unmethylated p54^{nrb} (Figs. 4, 5), which in turn could lead to the nuclear retention of mRNAs containing IR*Alu*s within paraspeckles. Moreover, it has been reported that p54^{nrb} can bind DNA through its C terminus (Yang et al. 1993). Consistent with this view, we demonstrated that the selective binding of dsRNAs to p54^{nrb} also requires its coiled-coil domain (Fig. 5).

Post-translational modifications of proteins play key roles in the regulation of many cellular processes by altering their associated effectors, including both proteins and a few reported RNAs. For instance, methylation/demethylation of Polycomb 2 protein could modulate its interaction with different lncRNAs (either TUG1 or MALAT1) with an unknown mechanism, resulting in the coordinated gene expression program in distinct subnuclear architectural compartments in response to growth signals (Yang et al. 2011). We observed that CARM1 methylation on p54^{nrb} occurs at or near the dsRNA-binding coiled-coil domain and that knockdown of CARM1 significantly alters p54^{nrb}-binding activity to dsRNAs but not ssRNAs (Fig. 5), resulting in enhanced nucleocytoplasmic export of mRNAs containing inverted *Alu* repeats. Thus, this regulation pathway represents one of a few examples where post-translational modification of an RNA-binding protein affects protein–RNA interaction and gene expression. Furthermore, although our data support the view that the reduced binding capability of methylated p54^{nrb} to dsRNAs could result from a direct conformational change of p54^{nrb} methylation at the coiled-coil domain, we cannot exclude the possibility that these methyl sites may recruit other effector proteins to facilitate the release of mRNA-IR*Alu*s from methylated p54^{nrb} (Yang et al. 2014). Finally, the dsRNA-binding protein STAU1 (Wickham et al. 1999) was recently shown to compete with p54^{nrb} for the binding of 3′ UTR IR*Alu*s, independent of editing (Elbarbary et al. 2013). It will be of interest to examine whether the binding of 3′ UTR IR*Alu*s with STAU1 occurs after the release of mRNAs containing IR*Alu*s from methylated p54^{nrb}.

Although many lncRNAs have been implicated in gene regulation and mammalian development (Ulitsky and Bartel 2013), how the expression of lncRNAs is regulated has remained poorly understood. Interestingly, we found that paraspeckle-localized CARM1 also plays a role in the transcription regulation of *NEAT1* RNAs and affects paraspeckle formation (Fig. 6). CARM1 is recognized as a transcriptional coactivator (Chen et al. 1999; Bedford and Clarke 2009) but also acts as a transcriptional cosuppressor, such as in the cyclic adenosine monophosphate signaling pathway (Xu et al. 2001). In the case of *NEAT1* regulation, we found that CARM1 is enriched at the *NEAT1* promoter and acts as a transcriptional repressor (Fig. 6). Conspicuously, this "negative" regulation of *NEAT1* transcription and paraspeckle formation by CARM1 could in fact lead to a "positive" gene expression output by allowing the export of more mRNAs with IR*Alu*s to the cytoplasm for protein translation. This final output in gene expression is therefore consistent with a general role of CARM1 in promoting gene transcription (Chen et al. 1999; Bedford and Clarke 2009). However, we do not yet know what directs CARM1 to the *NEAT1* promoter and what other factors are involved in this *NEAT1* transcription regulation by CARM1. It had been reported recently that *NEAT1* RNAs can sequester the transcriptional regulator PSF to regulate gene expression (Hirose et al. 2014; Imamura et al. 2014). Since PSF is largely localized to paraspeckles, it will be of interest to examine whether PSF can autoregulate *NEAT1* transcription in coordination with CARM1.

The identification of CARM1 functioning at two levels within paraspeckles is particularly interesting. On the one hand, CARM1 methylates p54^{nrb}, resulting in the reduced ability to binding to mRNAs containing IR*Alu*s (Figs. 3–5). On the other hand, CARM1 suppresses *NEAT1* transcription and paraspeckle formation (Figs. 6, 7I). Actions of CARM1 at these two levels synergistically work together to regulate the export of transcripts containing IR*Alu*s from paraspeckles. In response to certain cellular stressors, such as poly(I:C) treatment, we observed the reduced p54^{nrb} methylation (enhanced mRNA nuclear retention) and the decreased binding of CARM1 to the *NEAT1* promoter (enhanced transcription of *NEAT1* and paraspeckle formation) (Fig. 7A–F). Thus, this paraspeckle-mediated nuclear retention was enhanced upon poly(I:C) stimulation, leading to less translation of mRNAs containing IR*Alu*s (Fig. 7I).

Materials and methods

Cell culture, plasmids, transfection, and knockdown with shRNAs

HeLa, HEK293, and MEF cell lines were cultured using standard protocols. HEK293 CARM1 Flp-in stable cell line, wide-type, and CARM1$^{-/-}$ MEFs have been described (Cheng et al. 2007). Transfection was carried out with either X-tremeGENE 9 (Roche) or Lipofectamine 2000 (Invitrogen) according to the manufacturers' protocols. To generate Flag-p54^{nrb}-wt (MUT) or Flag-EGFP stable cell lines, pcDNA3.1 (+)-Flag-p54^{nrb}-wt (MUT) or pcDNA3.1 (+)-Flag-EGFP was transfected into HEK293 CARM1 Flp-in cells followed by G418 selection. The plasmids pEGFP-SC-Nicn1-*Alu* (IR*Alu*s) and pEGFP-SC-Lin28-*Alu* (IR*Alu*s) have been described (Chen et al. 2008). CARM1 knockdown was carried out as described (Ou et al. 2011), and stable HeLa and HEK293 lines were generated. To knock down p54^{nrb}, the sequence "GCAGG CGAAGTCTTCATTCAT" was inserted into pLVTHM vector with Mlu1 and Cla1, and the construct was packaged into lentivirus to infect HeLa cells. All plasmids used are listed in the Supplemental Material.

In vitro methylation assay

In vitro methylation assay was carried out as described (Cheng et al. 2007). GST-CARM1 and His-p54^{nrb} were overexpressed

and purified from *E. coli*. In vitro methylation reactions were performed in a final volume of 30 µL of PBS (pH 7.4). The reaction contained 0.5–1.0 µg of substrates and 0.2–0.4 µg of recombinant enzymes. All methylation reactions were carried out in the presence of 0.5 µCi S-adenosyl-L-[methyl-^{3}H] methionine (85 Ci/mmol from a 0.5 mCi/mL stock solution; Perkin-Elmer). The reaction was incubated for 1 h at 30°C and then subjected to fluorography by separation on SDS-PAGE (12% gel), transferred to a PVDF membrane, treated with Enhance (Perkin-Elmer), and exposed to film overnight. After in vitro methylation followed by fluorography, the same membrane was subjected to Coomassie blue staining, immunoblotting with anti-His tag, or Ponceau staining. We overlaid the fluorograph with the stained membrane and signals from immunoblots and verified that the stained protein bands matched with the methylated bands.

Immunoprecipitation

HeLa cells (10^7) were harvested and suspended in immunoprecipitation buffer (50 mM HEPES at pH 7.6, 250 mM NaCl, 5 mM EDTA at pH 8.0, 0.1% NP-40, 1 mM PMSF, protease inhibitor cocktail) followed by sonication. After centrifuging at 13,000 rpm for 15 min at 4°C, the supernatant was transferred into a new tube and precleared with 10 µL of Dynabeads G. Next, the precleared supernatant was incubated with 20 µL of Dynabeads G with antibodies for p54^{nrb} (BD) or IgG (Sigma) for 4 h at 4°C followed by washing with immunoprecipitation buffer. To harvest the protein complex, 50 µL of 1× SDS loading buffer (62.4 mM Tris at pH 6.8, 10% glycerol, 2% SDS, 0.0012% bromophenol blue) was added, incubated for 10 min at 95°C, and analyzed by Western blotting.

MS for methylation

pcDNA3.1 (+)-Flag- p54^{nrb} was transfected into scramble and CARM1 knockdown stable HeLa cells for 24 h, and cells transfected with Flag-EGFP were used as control. Cells (10^7) were harvested as described above, and 20 µL of anti-Flag M2 beads (Sigma) was used in each reaction. One out of 10 immunoprecipitated beads was saved for Western blotting and silver staining, and the others were used for MS. Beads were washed with PBS and then aliquoted into three parts (one each for Glu-C, substilisin, and trypsin digestion) followed by incubation with DTT and urea for 30 min at 60°C. Next, 15 mM iodoacetamide was added into the beads and incubated for 20 min at room temperature. Digestion was performed using sequencing grade Glu-C, substilisin, and trypsin for 4 h at 37°C. Liquid chromatography-tandem MS (LC-MS/MS) was carried out on the Thermo Q Exactive Hybrid quadrupole orbitrap mass spectrometer.

Nuclear and cytoplasmic RNA fractionation, RNA isolation, qRT–PCR, and Northern blotting

Nuclear and cytoplasmic fractionation was carried out as described (Chen et al. 2008) with slight modifications. Cell pellets were suspended by gentle pipetting in 200 µL of lysis buffer (10 mM Tris at pH 8.0, 140 mM NaCl, 1.5 mM $MgCl_2$, 0.5% Igepal, 2 mM vanadyl ribonucleoside complex [VRC]) and incubated for 5 min on ice. One-fifth of the lysate was saved as total RNA. The rest of the lysate was centrifuged at 1000*g* for 3 min at 4°C to pellet the nuclei, and the supernatant was the cytoplasmic fraction. To obtain pure cytoplasmic RNA, the supernatant fraction was further centrifuged at 13,000 rpm for 10 min at 4°C and then collected carefully to a new tube, and RNA was extracted with Trizol. To obtain pure nuclear RNA, the nuclear pellets were subjected to two additional washes with 160 µL of lysis buffer and one additional wash by adding 0.5% deoxycholic acid into the lysis buffer. Finally, the purified nuclei were resuspended in 100 µL of lysis buffer followed by extraction with Trizol. The RNA was extracted per standard protocols. For Northern blotting, equal amounts of RNAs from different fractionations were loaded. Northern blotting was performed using the DIG Northern starter kit (Roche). The probes used were produced by digoxigenin (Dig)-labeled in vitro transcription (IVT) of specific PCR products. Primers used for amplifying templates for IVT are listed in the Supplemental Material. For qRT–PCR, after treatment with DNase I (Ambion), equal amounts of RNAs from different fractionations were reverse-transcribed into cDNAs with SuperScript II (Invitrogen). β-Actin was used as an endogenous control.

RNA ISH and immunofluorescence microscopy

Simultaneous RNA ISH and immunofluorescence were performed as described (Yin et al. 2012) with slight modifications. Hybridization was performed with in vitro transcribed Dig-labeled probes. For colocalization studies, cells were costained with mouse anti-p54^{nrb} (BD) and/or rabbit anti-CARM1 (Bethyl Laboratories). The nuclei were counterstained with DAPI. Images were taken with a Zeiss LSM 510 microscope or an Olympus IX70 DeltaVision RT deconvolution system microscope. For statistical analysis, >300 cells from each group were observed and calculated. Image analyses of signal intensity were carried out by Image-Pro Plus according to standard protocols and were described previously (Yin et al. 2015).

Formaldehyde cross-linking RIP

HeLa cells (10^7) were washed twice with 5 mL of PBS and cross-linked with 1% formaldehyde for 10 min at room temperature. Cross-linking was stopped by the addition of glycine to a final concentration of 0.25 M followed by incubation for 5 min at room temperature. After washing twice with 5 mL of cold PBS, cells were collected and suspended in 1 mL of RIP buffer (50 mM Tris-HCl at pH 7.5, 150 mM NaCl, 1% NP40, 0.5% sodium deoxycholate, 1 mM PMSF, 2 mM VRC, protease inhibitor cocktail). The cells were homogenized by sonication and then centrifuged at 13,000 rpm for 10 min at 4°C to remove the insoluble material. Fifty microliters of supernatant was saved as input. The rest of the supernatant was precleared by applying 10 µL of Dynabeads G (Invitrogen) with 20 µg/mL yeast tRNA for 1 h at 4°C. Next, the precleared lysate was incubated with Dynabeads G that were precoated with 2 µg of antibodies for p54^{nrb} (BD) or IgG (Sigma) for 4 h at 4°C. The beads were washed three times for 5 min with washing buffer I (50 mM Tris-HCl at pH 7.5, 1 M NaCl; 1% NP40, 1% sodium deoxycholate, 2 mM VRC) and three times for 5 min with washing buffer II (50 mM Tris-HCl at pH 7.5, 1 M NaCl, 1% NP40, 1% sodium deoxycholate, 2 mM VRC, 1 M urea). The immunoprecipitated complex was eluted from Dynabeads G by adding 100 µL of elution buffer (100 mM Tris HCl at pH 8.0, 10 mM EDTA, 1% SDS). Proteinase K (0.2 µg/µL) and 200 mM NaCl were added into the RNA sample and incubated for 1 h at 42°C followed by 1 h at 65°C. RNA was then extracted, digested with DNase I (Ambion), and used to synthesize cDNA using random hexamers (SuperScript III, Invitrogen) followed by qPCR analysis (AceQ, Vazyme).

UV cross-linking RIP

UV cross-linking RIP was carried out as described (Zhang et al. 2013b). HeLa cells (10^7) were washed twice with 5 mL of cold

PBS and irradiated at 150 mJ/cm^2 at 254 nm in a Stratalinker. Cells were collected and resuspended in 1 mL of RIP buffer. The cells were homogenized by sonication and then centrifuged at 13,000 rpm for 10 min at 4°C to remove the insoluble material. Fifty microliters of supernatant was saved as input. The rest of the supernatant was precleared by applying 10 µL of Dynabeads G (Invitrogen) with 20 µg/mL yeast tRNA for 1 h at 4°C. Next, the precleared lysate was incubated with Dynabeads G that were precoated with 2 µg of antibodies for p54^{nrb} (BD) or IgG (Sigma) for 4 h at 4°C. The beads were washed three times for 5 min with washing buffer I and three times for 5 min with washing buffer II. The immunoprecipitated complex was eluted from Dynabeads G by adding 100 µL of elution buffer (100 mM Tris-HCl at pH7.0, 5 mM EDTA, 10 mM DTT, 1% SDS). Five microliters of 10 mg/mL proteinase K was added into the RNA sample and incubated for 30 min at 55°C. RNA was then extracted, digested with DNase I (Ambion), and used to synthesize cDNA using random hexamers (SuperScript III, Invitrogen) followed by qPCR analysis.

ChIP

ChIP was carried out as described (Zhang et al. 2013b). HeLa cells (10^7) were cross-linked in 1% formaldehyde for 5 min at room temperature, quenched by adding 0.25 M glycine, and then collected by cell scraper. After being suspended in 1 mL of ChIP lysis buffer (1% Triton X-100, 0.1% sodium deoxycholate, 50 mM Tris at pH 8.0, 150 mM NaCl, 5 mM EDTA), cells were sonicated until the majority of DNA fragments was 300–500 base pairs (bp). Supernatants were collected and subjected to preclearing with Dynabeads G (Invitrogen) with a supplement of 100 µg of ssDNA. Next, the precleared lysates were used for ChIP with 2 µg of CARM1 antibody (Bethyl Laboratories). ChIP was carried out overnight at 4°C. The beads were washed with 600 µL of ChIP lysis buffer, 600 µL of high-salt wash buffer (1% Triton X-100, 0.1% deoxycholate, 50 mM Tris at pH 8.0, 500 mM NaCl, 5 mM EDTA), and 600 µL of LiCl immune complex wash buffer (0.25 M LiCl, 0.5% Igepal, 0.5% deoxycholate, 10 mM Tris at pH 8.0, 1 mM EDTA) sequentially followed by two washes with 600 µL of 1× TE buffer (10 mM Tris at pH 8.0, 1 mM EDTA) at 4°C. The immunoprecipitated complex was eluted from Dynabeads G by adding 200 µL of fresh-prepared elution buffer (1% SDS, 0.1 M $NaHCO_3$) with rotation for 15 min at room temperature. Next, the reverse cross-linking was carried out by adding 8 µL of 5 M NaCl and incubation for 4 h at 65°C followed by the addition of 4 µL of 0.5 M EDTA and 10 µL of 10 mg/mL proteinase K for 2 h at 55°C. DNA was then extracted and analyzed by qPCR.

NRO assay

The NRO in HeLa cells was performed as described (Zhang et al. 2013b). HeLa cells (10^7) were washed with cold PBS three times and incubated in swelling buffer (10 mM Tris at pH 7.5, 2 mM $MgCl_2$, 3 mM $CaCl_2$) for 5 min on ice. Cells were collected, suspended in 1.5 mL of lysis buffer (10 mM Tris at pH 7.5, 2 mM $MgCl_2$, 3 mM $CaCl_2$, 0.5% Igepal, 10% glycerol, 2 U/mL RNasin ribonuclease inhibitor [Promega]), gently pipetted, and then centrifuged at 1500*g* for 10 min at 4°C. The pellets were collected and subjected to another lysis to obtain purer nuclei. The resulting nuclear pellets were resuspended in 100 µL of NRO buffer (50 mM Tris at pH 7.5, 5 mM $MgCl_2$, 150 mM KCl, 0.1% sarkosyl, 2 U/mL RNase inhibitor, 10 mM DTT) containing 0.1 mM ATP, GTP, CTP, and BrUTP (Sigma). Transcription was performed for 3 min on ice and then 5 min at room temperature. The reaction was stopped by addition of 600 µL of Trizol reagent, and RNA was extracted followed by the DNase I (Ambion) treatment to remove genomic DNA. The purified RNAs were incubated with 2 µg of anti-BrdU antibody (Sigma) or an equal amount of IgG antibody (Sigma) for 2 h at 4°C and then immunoprecipitated for 1 h with Dynabeads Protein G (Invitrogen) precoated with yeast tRNA (Sigma). Precipitated RNAs were extracted by Trizol reagent and used for cDNA synthesis and qPCR analysis. All measured samples were normalized to β-*actin* transcription.

Biotin-labeled RNA pull-down

Biotinylated RNA pull-down assays were performed as described (Zhang et al. 2013b). DNA fragments of full-length EGFP with T7 promoter on its 5′ end and fragment EGFP (76–495) with T7 promoters on both ends were in vitro transcribed with the biotin RNA-labeling mix (Roche) and T7 transcription kit (Promega). HeLa cells (10^7) were collected and suspended in 1 mL of RIP buffer (25 mM Tris at pH 7.5, 150 mM KCl, 0.5 mM DTT, 0.5% NP40, 1 mM PMSF, 2 mM VRC, protease inhibitor cocktail) followed by sonication. After being centrifuged at 13,000 rpm for 15 min at 4°C, the supernatant was transferred into a new tube and precleared with 40 µL of streptavidin Dynabeads for 20 min at 4°C. Next, 20 µg/mL yeast tRNA was added to block unspecific binding and incubated for 20 min at 4°C. The precleared lysate was divided into two parts, and each was supplemented with 2 µg of biotin-labeled *ss_egfp* (full length of egfp) or *ds_egfp* (an inverted repeated fragment of *egfp*) and incubated for 1.5 h followed by addition of 40 µL of streptavidin Dynabeads and incubation for another 1.5 h at room temperature. Beads were washed four times for 5 min with RIP buffer containing 0.5% sodium deoxycholate and boiled in 1× SDS loading buffer for 10 min at 100°C. The retrieved proteins were analyzed by Western blotting with anti-p54^{nrb} (BD), anti-methyl-p54^{nrb} (620me), and anti-PSF (Sigma).

tRSA RNA pull-down

tRSA RNA pull-down assays were carried out as described (Iioka et al. 2011) with modifications. IR*Alu*s from the 3′ UTR of *Nicn1* were cloned into pcDNA3 with the tRSA tag at its 5′end. tRSA-IR*Alu*s or tRSA was in vitro transcribed using the T7 transcription kit (Promega). Ten micrograms per reaction of synthetic RNAs was denatured for 5 min at 65°C and cooled to room temperature in the presence of PA buffer (10 mM Tris at pH 7.4, 10 mM $MgCl_2$, 100 mM NH_4Cl). Next, the RNAs were incubated with 40 µL of streptavidin Dynabeads for 20 min at 4°C in the presence of 2 U/mL RNasin (Promega). HeLa cells (10^7) were collected and resuspended in 1 mL of lysis buffer (25 mM Tris at pH 7.4, 150 mM KCl, 0.5 mM DTT, 0.5% NP40, 1 mM PMSF, 2 mM VRC, protease inhibitor cocktail) followed by sonication. After centrifuging at 13,000 rpm for 15 min 4°C, the supernatant was transferred into a new tube and precleared with 40 µL of streptavidin Dynabeads for 20 min at 4°C followed by the addition of 20 µg/mL yeast tRNA for 20 min at 4°C. Beads prebound with tRSA-IR*Alu*s RNA or tRSA RNA were incubated with precleared lysates for 4 h at 4°C followed by washing with lysis buffer containing 0.5% sodium deoxycholate. To harvest the protein complex, 50 µL of 1× SDS loading buffer was added and incubated for 10 min at 95°C and then analyzed by Western blotting.

Dig-labeled RNA pull-down

Dig-RNA pull-down assays were carried out as described (Arab et al. 2014) with modifications. Two 10-cm dishes of cells expressing Flag-p54^{nrb}-wt (MUT) or Flag-EGFP were used to immunoprecipitate with anti-Flag M2 (20 µL for each reaction) (Sigma). After immunoprecipitation and washing, one out of five beads was saved for Western blot. The rest were equilibrated in binding buffer (50 mM Tris at pH 8.0, 10% glycerol, 100 mM KCl, 5 mM

$MgCl_2$, 10 mM β-mercaptoethanol, 0.1% NP-40) and incubated with 200 ng of Dig-labeled RNA in binding buffer for 1.5 h at room temperature. The Dig-labeled RNA was produced by Dig-labeled IVT of an IR*Alu*s DNA fragment, which was amplified from the 3′ UTR of *Nicn1*. After washing with immunoprecipitation buffer containing 500 mM NaCl, the bound RNA was extracted and analyzed by Northern blotting.

*Computational pipeline for the analysis of genes containing 3′ UTR IR*Alus *enriched in the* NEAT1 *DNA CHART*

A stringent pipeline was developed to identify 3′ UTR IR*Alu*s genes enriched by *NEAT1* DNA CHART. To identify 3′ UTR IR*Alu*s genes, IR*Alu*s were identified by RepeatMasker (Tarailo-Graovac and Chen 2009). The 3′ UTRs were defined in a RefSeq gene file. Next, the overlap region between IR*Alu*s and the 3′ UTR was calculated to ensure that IR*Alu*s were located in the 3′ UTRs. In total, 545 genes containing 3′ UTR IR*Alu*s were obtained. In MCF7 cells, 388 genes containing 3′ UTR IR*Alu*s were expressed (reads per kilobase per million mapped reads [RPKM] ≥ 2) by analyzing the available RNA sequencing data sets (MCF7 RNA-seq; Gene Expression Omnibus [GEO]: GSE47042) (Janky et al. 2014). To analyze the *NEAT1* DNA CHART-enriched IR*Alu*s-containing genes, the *NEAT1* DNA CHART-seq data sets carried out in MCF7 cells (GEO: GSE47042) (West et al. 2014) were used to call peaks by MACS (version 1.4.2, 20120305) (Feng et al. 2012). One-hundred-forty-nine MCF cells expressed genes that contain 3′ UTR IR*Alu*s enriched by the *NEAT1* DNA CHART.

Acknowledgments

We are grateful to G. Carmichael for critical reading of the manuscript, M.R. Stallcup for CARM1 shRNA, and M. Person for MS analysis at the Protein and Metabolite Analysis Facility (University of Texas, Austin) supported by RP110782 (Cancer Prevention Research Institute of Texas). This work is supported by grants 91440202 and 31322018 from the Natural Science Foundation of China (NSFC), and XDA01010206 from Chinese Academy of Sciences (CAS) to L.-L.C.; 31271390 from NSFC to L.Y; and DK062248 from National Institutes of Health to M.T.B. M.T.B. is a cofounder of EpiCypher.

References

Arab K, Park YJ, Lindroth AM, Schafer A, Oakes C, Weichenhan D, Lukanova A, Lundin E, Risch A, Meister M, et al. 2014. Long noncoding RNA TARID directs demethylation and activation of the tumor suppressor TCF21 via GADD45A. *Mol Cell* **55:** 604–614.

Bedford MT, Clarke SG. 2009. Protein arginine methylation in mammals: who, what, and why. *Mol Cell* **33:** 1–13.

Bond CS, Fox AH. 2009. Paraspeckles: nuclear bodies built on long noncoding RNA. *J Cell Biol* **186:** 637–644.

Chen LL, Carmichael GG. 2008. Gene regulation by SINES and inosines: biological consequences of A-to-I editing of *Alu* element inverted repeats. *Cell Cycle* **7:** 3294–3301.

Chen LL, Carmichael GG. 2009. Altered nuclear retention of mRNAs containing inverted repeats in human embryonic stem cells: functional role of a nuclear noncoding RNA. *Mol Cell* **35:** 467–478.

Chen D, Ma H, Hong H, Koh SS, Huang SM, Schurter BT, Aswad DW, Stallcup MR. 1999. Regulation of transcription by a protein methyltransferase. *Science* **284:** 2174–2177.

Chen SL, Loffler KA, Chen D, Stallcup MR, Muscat GE. 2002. The coactivator-associated arginine methyltransferase is necessary for muscle differentiation: CARM1 coactivates myocyte enhancer factor-2. *J Biol Chem* **277:** 4324–4333.

Chen LL, DeCerbo JN, Carmichael GG. 2008. *Alu* element-mediated gene silencing. *EMBO J* **27:** 1694–1705.

Cheng D, Cote J, Shaaban S, Bedford MT. 2007. The arginine methyltransferase CARM1 regulates the coupling of transcription and mRNA processing. *Mol Cell* **25:** 71–83.

Clemson CM, Hutchinson JN, Sara SA, Ensminger AW, Fox AH, Chess A, Lawrence JB. 2009. An architectural role for a nuclear noncoding RNA: *NEAT1* RNA is essential for the structure of paraspeckles. *Mol Cell* **33:** 717–726.

Elbarbary RA, Li W, Tian B, Maquat LE. 2013. STAU1 binding 3′ UTR IR*Alu*s complements nuclear retention to protect cells from PKR-mediated translational shutdown. *Genes Dev* **27:** 1495–1510.

Feng J, Liu T, Qin B, Zhang Y, Liu XS. 2012. Identifying ChIP-seq enrichment using MACS. *Nat Protoc* **7:** 1728–1740.

Fox AH, Lam YW, Leung AK, Lyon CE, Andersen J, Mann M, Lamond AI. 2002. Paraspeckles: a novel nuclear domain. *Curr Biol* **12:** 13–25.

Fox AH, Bond CS, Lamond AI. 2005. $P54^{nrb}$ forms a heterodimer with PSP1 that localizes to paraspeckles in an RNA-dependent manner. *Mol Biol Cell* **16:** 5304–5315.

Hirose T, Virnicchi G, Tanigawa A, Naganuma T, Li R, Kimura H, Yokoi T, Nakagawa S, Benard M, Fox AH, et al. 2014. NEAT1 long noncoding RNA regulates transcription via protein sequestration within subnuclear bodies. *Mol Biol Cell* **25:** 169–183.

Hundley HA, Krauchuk AA, Bass BL. 2008. *C. elegans* and *H. sapiens* mRNAs with edited 3′ UTRs are present on polysomes. *RNA* **14:** 2050–2060.

Iioka H, Loiselle D, Haystead TA, Macara IG. 2011. Efficient detection of RNA–protein interactions using tethered RNAs. *Nucleic Acids Res* **39:** e53.

Imamura K, Imamachi N, Akizuki G, Kumakura M, Kawaguchi A, Nagata K, Kato A, Kawaguchi Y, Sato H, Yoneda M, et al. 2014. Long noncoding RNA NEAT1-dependent SFPQ relocation from promoter region to paraspeckle mediates IL8 expression upon immune stimuli. *Mol Cell* **53:** 393–406.

Janky R, Verfaillie A, Imrichova H, Van de Sande B, Standaert L, Christiaens V, Hulselmans G, Herten K, Naval Sanchez M, Potier D, et al. 2014. iRegulon: from a gene list to a gene regulatory network using large motif and track collections. *PLoS Comput Biol* **10:** e1003731.

Lee J, Bedford MT. 2002. PABP1 identified as an arginine methyltransferase substrate using high-density protein arrays. *EMBO Rep* **3:** 268–273.

Lee YH, Koh SS, Zhang X, Chen X, Stallcup MR. 2002. Synergy among nuclear receptor coactivators: selective requirement for protein methyltransferase and acetyltransferase activities. *Mol Cell Biol* **22:** 3621–3632.

Li J, Zhao Z, Carter C, Ehrlich LI, Bedford MT, Richie ER. 2013. Coactivator-associated arginine methyltransferase 1 regulates fetal hematopoiesis and thymocyte development. *J Immunol* **190:** 597–604.

Mao YS, Sunwoo H, Zhang B, Spector DL. 2011a. Direct visualization of the co-transcriptional assembly of a nuclear body by noncoding RNAs. *Nat Cell Biol* **13:** 95–101.

Mao YS, Zhang B, Spector DL. 2011b. Biogenesis and function of nuclear bodies. *Trends Genet* **27:** 295–306.

Naganuma T, Nakagawa S, Tanigawa A, Sasaki YF, Goshima N, Hirose T. 2012. Alternative 3′-end processing of long

noncoding RNA initiates construction of nuclear paraspeckles. *EMBO J* **31:** 4020–4034.

Ou CY, LaBonte MJ, Manegold PC, So AY, Ianculescu I, Gerke DS, Yamamoto KR, Ladner RD, Kahn M, Kim JH, et al. 2011. A coactivator role of CARM1 in the dysregulation of β-catenin activity in colorectal cancer cell growth and gene expression. *Mol Cancer Res* **9:** 660–670.

Prasanth KV, Prasanth SG, Xuan Z, Hearn S, Freier SM, Bennett CF, Zhang MQ, Spector DL. 2005. Regulating gene expression through RNA nuclear retention. *Cell* **123:** 249–263.

Saha S, Murthy S, Rangarajan PN. 2006. Identification and characterization of a virus-inducible non-coding RNA in mouse brain. *J Gen Virol* **87:** 1991–1995.

Sasaki YT, Ideue T, Sano M, Mituyama T, Hirose T. 2009. MENε/β noncoding RNAs are essential for structural integrity of nuclear paraspeckles. *Proc Natl Acad Sci* **106:** 2525–2530.

Sunwoo H, Dinger ME, Wilusz JE, Amaral PP, Mattick JS, Spector DL. 2009. MENε/β nuclear-retained non-coding RNAs are upregulated upon muscle differentiation and are essential components of paraspeckles. *Genome Res* **19:** 347–359.

Tarailo-Graovac M, Chen N. 2009. Using RepeatMasker to identify repetitive elements in genomic sequences. *Curr Protoc Bioinformatics* **C25:** 4.10.1–4.10.14.

Ulitsky I, Bartel DP. 2013. lincRNAs: genomics, evolution, and mechanisms. *Cell* **154:** 26–46.

West JA, Davis CP, Sunwoo H, Simon MD, Sadreyev RI, Wang PI, Tolstorukov MY, Kingston RE. 2014. The long noncoding RNAs NEAT1 and MALAT1 bind active chromatin sites. *Mol Cell* **55:** 791–802.

Wickham L, Duchaine T, Luo M, Nabi IR, DesGroseillers L. 1999. Mammalian staufen is a double-stranded-RNA- and tubulin-binding protein which localizes to the rough endoplasmic reticulum. *Mol Cell Biol* **19:** 2220–2230.

Xu W, Chen H, Du K, Asahara H, Tini M, Emerson BM, Montminy M, Evans RM. 2001. A transcriptional switch mediated by cofactor methylation. *Science* **294:** 2507–2511.

Yadav N, Cheng D, Richard S, Morel M, Iyer VR, Aldaz CM, Bedford MT. 2008. CARM1 promotes adipocyte differentiation by coactivating PPARγ. *EMBO Rep* **9:** 193–198.

Yang YS, Hanke JH, Carayannopoulos L, Craft CM, Capra JD, Tucker PW. 1993. NonO, a non-POU-domain-containing, octamer-binding protein, is the mammalian homolog of Drosophila nonAdiss. *Mol Cell Biol* **13:** 5593–5603.

Yang Y, Lu Y, Espejo A, Wu J, Xu W, Liang S, Bedford MT. 2010. TDRD3 is an effector molecule for arginine-methylated histone marks. *Mol Cell* **40:** 1016–1023.

Yang L, Lin C, Liu W, Zhang J, Ohgi Kenneth A, Grinstein Jonathan D, Dorrestein Pieter C, Rosenfeld Michael G. 2011. ncRNA- and Pc2 methylation-dependent gene relocation between nuclear structures mediates gene activation programs. *Cell* **147:** 773–788.

Yang Y, McBride KM, Hensley S, Lu Y, Chedin F, Bedford MT. 2014. Arginine methylation facilitates the recruitment of TOP3B to chromatin to prevent R loop accumulation. *Mol Cell* **53:** 484–497.

Yin QF, Yang L, Zhang Y, Xiang JF, Wu YW, Carmichael GG, Chen LL. 2012. Long noncoding RNAs with snoRNA ends. *Mol Cell* **48:** 219–230.

Yin QF, Hu SB, Xu YF, Yang L, Carmichael GG, Chen LL. 2015. snoVectos for nuclear expression of RNA. *Nucleic Acids Res* **43:** e5.

Zhang Z, Carmichael GG. 2001. The fate of dsRNA in the nucleus: a p54(^{nrb})-containing complex mediates the nuclear retention of promiscuously A-to-I edited RNAs. *Cell* **106:** 465–475.

Zhang Q, Chen CY, Yedavalli VS, Jeang KT. 2013a. NEAT1 long noncoding RNA and paraspeckle bodies modulate HIV-1 posttranscriptional expression. *mBio* **4:** e00596–00512.

Zhang Y, Zhang XO, Chen T, Xiang JF, Yin QF, Xing YH, Zhu S, Yang L, Chen LL. 2013b. Circular intronic long noncoding RNAs. *Mol Cell* **51:** 792–806.

Zhao R, Bodnar MS, Spector DL. 2009. Nuclear neighborhoods and gene expression. *Curr Opin Genet Dev* **19:** 172–179.

Protein arginine methyltransferase CARM1 attenuates the paraspeckle-mediated nuclear retention of mRNAs containing IR *Alu*s

Shi-Bin Hu, Jian-Feng Xiang, Xiang Li, et al.

Genes Dev. 2015 29: 630-645
Access the most recent version at doi:10.1101/gad.257048.114

Inventory of Supplemental Information

I. Supplemental Figures

Supplemental Figure S1-S2 is related to main Figure 1.

Supplemental Figure S3-S6 is related to main Figure 2.

Supplemental Figure S5 is related to main Figures 2, 4, 5, 7.

Supplemental Figure S7 is related to main Figure 3.

II. Supplemental Tables

Supplemental Table S1 includes all primer sequences used in the study.

Supplemental figure legends

Figure S1. Characterization of p54^{nrb} methylation (related to Figure 1). (A) Identification of p54^{nrb} methylation by PRMTs. The indicated PRMTs were used to methylate p54^{nrb}. The methylated proteins were separated by SDS-PAGE, transferred to a PVDF membrane, and visualized by fluorography. The same membrane was subjected to Ponceau staining to verify substrate equal loading. (B) Characterization of p54^{nrb} methylation by CARM1. Top, a schematic view of regions of p54^{nrb} fused to his-tag for deletion analysis. Bottom, purified his-tagged p54^{nrb} truncations were incubated with recombinant GST-CARM1 in the presence of [^{3}H]AdoMet, separated by SDS-PAGE, and the methylated proteins visualized by fluorography (bottom right panel). A duplicate substrate gel was Coomassie stained to demonstrate loading (bottom left panel). Red dots indicated the expression of p54^{nrb} truncations.

Figure S2. p54^{nrb} is methylated by CARM1 (related to Figure 1). (A) CARM1 was knocked down in HeLa and HEK 293 cells, as validated by Western blotting (WB). Actin was used as a loading control. (B) Flag- p54^{nrb} was expressing in scramble and CARM1 KD HeLa cells. The top is the silver staining of IP complex. The bottom is the western blotting analysis of IP efficiency. The Flag-p54^{nrb} IP samples were subjected to MS. (C) The sequence of human p54^{nrb}. Amino Acids highlighted by blue indicate the RRM domains, while Amino Acids highlighted by red indicate the Coiled-coil domain. All Arginines (R) were underscored. R73, R184 and R207 were present in both scramble and CARM1 knockdown Flag-p54^{nrb} IP samples, while R357, R365 and R378 were present in the scramble, but not the CARM1 knockdown, Flag-p54^{nrb} IP sample. (D) Hybrid mass spectrometry identified Arg357, Arg365 and Arg378 are major methylation sites on p54^{nrb} by CARM1 in HeLa cells.

Figure S3. CARM1 deficiency suppresses *egfp*-IR*Alu*s expression (related to Figure 2). (A) CARM1 KD suppresses EGFP expression of *egfp* mRNA containing IR*Alu*s in its 3'-UTR. IR*Alu*s and *Alu* from the 3'-UTR of *Lin28* were inserted into the 3'-UTR of *egfp* mRNA (Chen et al. 2008). Stable HeLa cell lines with the scramble shRNA treatment and CARM1 KD were transfected with the indicated plasmids and fluorescence observed 24 h after transfection. (B) The expression of EGFP and transcripts of *egfp* from the same batch of transfected HeLa cells as described (A) were investigated by WB by probing with anti-EGFP antibody; and by NB by probing with a Dig-labeled *egfp* fragment. Actin was used as loading control for WB. Equivalent amounts of total RNAs were loaded for NB as indicated by 28S and 18S rRNAs. (C) The relative translation efficiency (the relative intensity of each corresponding band from WB and NB shown in panel B) of *egfp-Alu* and *egfp-IRAlus* mRNA in scramble and CARM1 KD cells.

Figure S4. CARM1 deficiency enhances nuclear retention of mRNAs containing IR*Alu*s in HEK293 cells (related to Figure 2). (A) CARM1 KD suppresses EGFP expression of *egfp* mRNA containing IR*Alu*s in its 3'-UTR. IR*Alu*s and *Alu* from the 3'-UTR of *Nicn1* were inserted into the 3'-UTR of *egfp* mRNA (Chen et al. 2008). Stable HEK293 cell lines with the scramble shRNA treatment and CARM1 KD were transfected with the indicated plasmids and fluorescence observed 24 h after transfection. (B) The expression of EGFP and transcripts of

egfp from the same batch of transfected HEK293 cells as described in (A) were investigated by WB by probing with anti-EGFP antibody. Actin was used as loading control for WB. (C) CARM1 deficiency significantly enhances the nuclear retention of *egfp* mRNA with IR*Alu*s. The cytoplasmic and nuclear RNAs were isolated from HEK293 cells with the indicted treatment and then were used for RT-qPCR analysis. Note that the sub-cellular distributions of both the co-transfected *mcherry* and the endogenous *actin* mRNAs exhibited little changes in the scramble and CARM1 KD HEK293 cells. (D) CARM1 KD enhances the nuclear retention of other endogenous mRNAs with IR*Alu*s in HEK293 cells. RT-qPCR analyzed a number of other endogenous mRNAs with IR*Alu*s using nuclear and cytoplasmic fractionated RNAs. Primers to detect IR*Alu*s RNAs were designed in the downstream of IR*Alu*s in 3'-UTRs (Figure S5). The relative subcellular distribution of each IR*Alu*s RNA was normalized to the relative amount of *malat1* RNA. In (C)(D), SD was obtained from three independent experiments. (*)P<0.05; (**)P<0.01; n=3.

Figure S5. A schematic drawing of transcripts containing a pair of IR*Alu*s in their 3'-UTRs (related to Figures 2, 4, 5 and 7). Black bars represent exons, thin black lines represent introns. The position and direction of *Alu* elements in 3'-UTRs were shown in white arrows. The primer set recognizing each transcript is labeled as a thick blue line underneath.

Figure S6. CARM1 KD enhances the nuclear retention of endogenous mRNAs with IR*Alu*s in their 3'-UTRs (related to Figure 2). (A) RT-qPCR quantitations of endogenous mRNAs with IR*Alu*s in total, cytoplasmic and nuclear fractionations. The level of each cellular mRNA was normalized to the level of *actin* mRNA in scramble and CARM1 KD HeLa cells. SD was obtained from three independent experiments. (*)P<0.05; (**)P<0.01; n=3. T, total RNA; C, cytoplasmic RNAs; N, nuclear RNAs. (B) CARM1 KD promotes the nuclear retention of endogenous *icmt* mRNA. Top, cytoplasmic and nuclear RNA fractionation of scramble and CARM1 KD HeLa cells followed by NB to detect *icmt* mRNA. $tRNA^{lys}$ and *actin* revealed a successful cytoplasmic and nuclear fractionation. Equivalent amounts of RNA from different compartments were loaded as indicated by 28S and 18S rRNAs. Bottom, the relative subcellular distribution of the *icmt* mRNA was quantified from top panels by Image J and was presented by the normalization to the *actin* mRNA in each subcellular compartment.

Figure S7. Visualization of *mcherry-IRAlus* expression after $p54^{nrb}$ and CARM1 knockdown (related to Figure 3). (A) While CARM1 KD suppresses mcherry expression of *mcherry* mRNA containing IR*Alu*s in its 3'-UTR, knockdown of $p54^{nrb}$ enhances mcherry expression of the same plasmid. (B) Expression of WT CARM1 but not the catalytic inactive mutant E266Q CARM1 in CARM1 KD HeLa cells could rescue the expression of mcherry mRNAs with IR*Alu*s in its 3'-UTR. (C) A schematic drawing for the nuclear retention regulation of *mcherry* mRNAs with IR*Alu*s in its 3'-UTR under different conditions. See text for details.

Supplemental figures

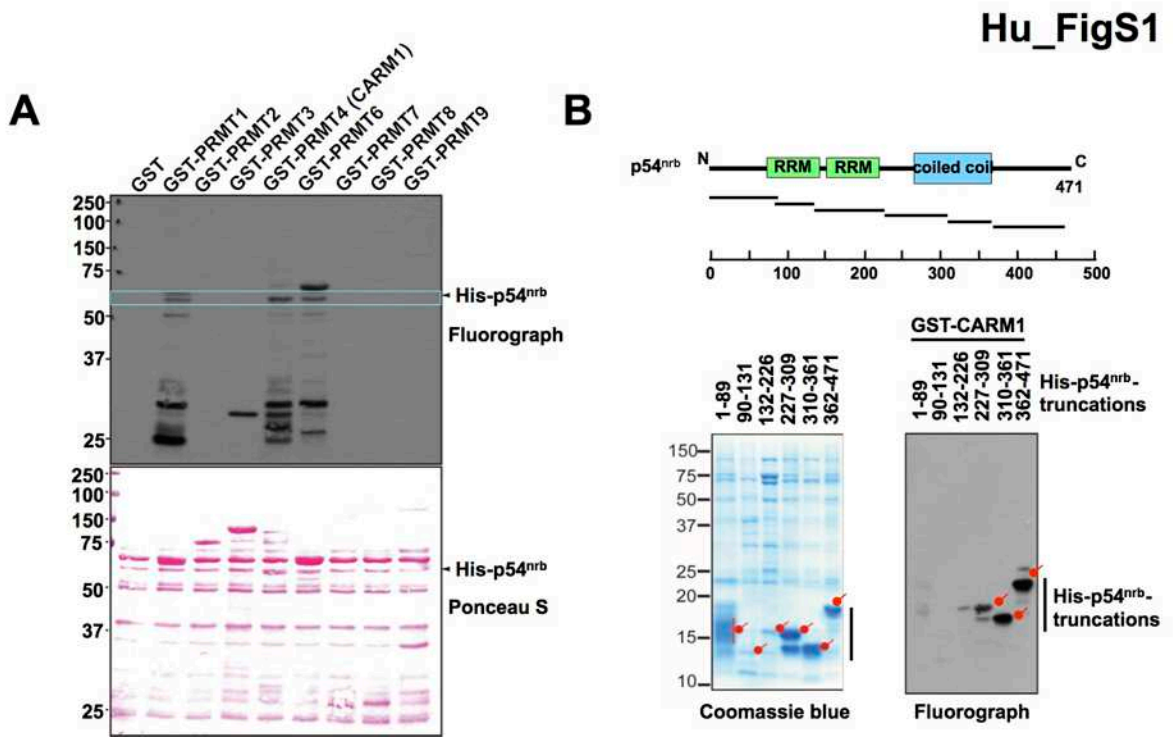

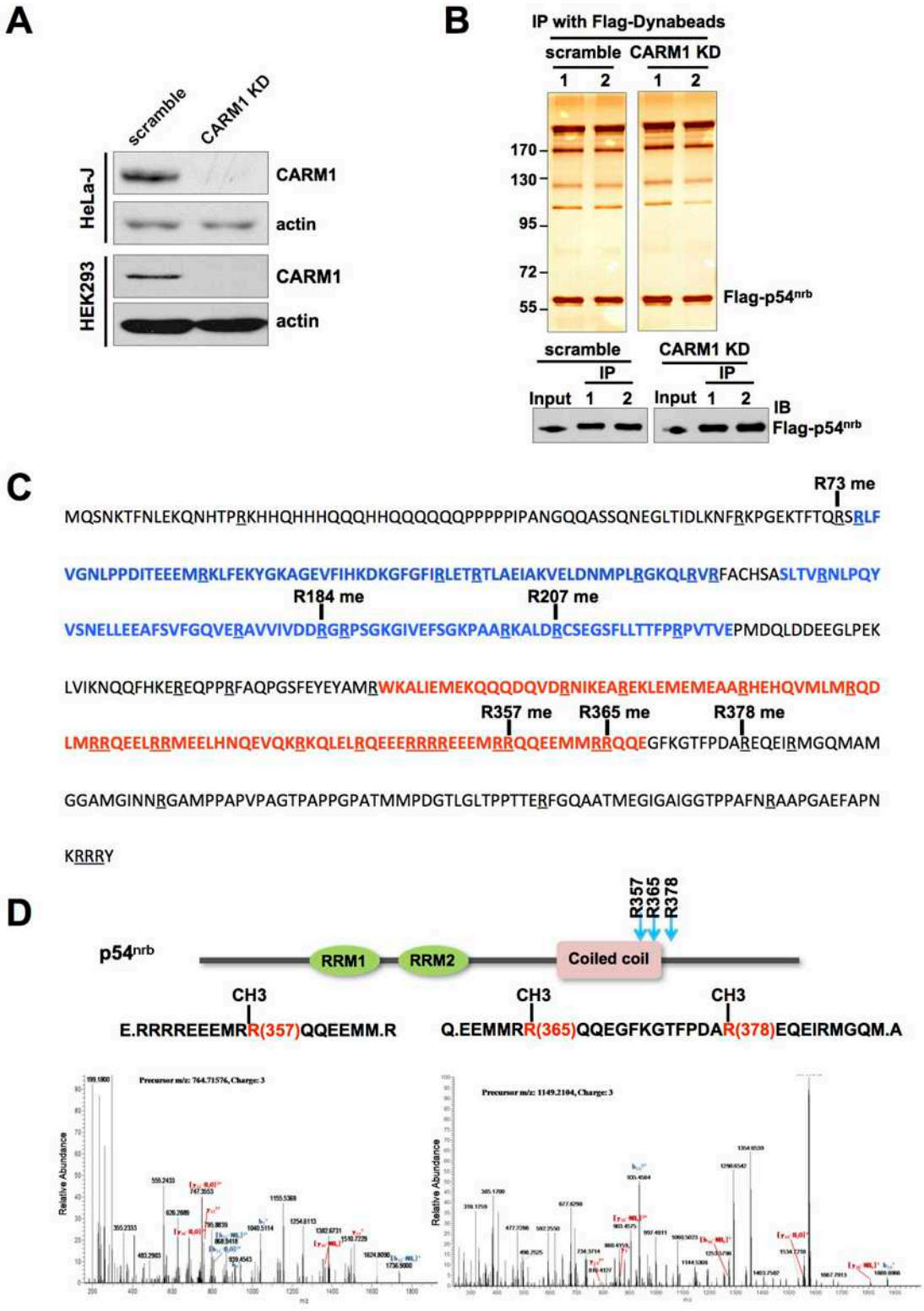
A
scramble
CARM1 KD
HeLaJ
CARM1
actin
HEK293
CARM1
actin
B
IP with Flag-Dynabeads
scramble
CARM1 KD
1 2 1 2
170
130
95
72
55
Flag-p54nrb
scramble
CARM1 KD
IP
IP
Input 1 2
Input 1 2
IB
Flag-p54nrb
C
R73 me
MQSNKTFNLEKQNHTPRKHHQHHHQQQHHQQQQQQPPPPPIPANGQQASSQNEGLTIDLKNFRKPGEKTFTQRSRLF
VGNLPPDITEEEMRKLFEKYGKAGEVFIHKDKGFGFIRLETRTLAEIAKVELDNMPLRGKQLRVRFACHSASLTVRNLPQY
R184 me
R207 me
VSNELLEEAFSVFGQVERAVVIVDDRGRPSGKGIVEFSGKPAARKALDRCSEGSFLLTTFPRPVTVEPMDQLDDEEGLPEK
LVIKNQQFHKEREQPPRFAQPGSFEYEYAMRWKALIEMEKQQQDQVDRNIKEAREKLEMEMEAARHEHQVMLMRQD
R357 me
R365 me
R378 me
LMRRQEELRRMEELHNQEVQKRKQLELRQEEERRRREEEMRRQQEEMMRRQQEGFKGTFPDAREQEIRMGQMAM
GGAMGINNRGAMPPAPVPAGTPAPPGPATMMPDGTLGLTPPTTERFGQAATMEGIGAIGGTPPAFNRAAPGAEFAPN
KRRRY
D
R357
R365
R378
p54nrb
RRM1
RRM2
Coiled coil
CH3
CH3
CH3
E.RRRREEEMRR(357)QQEEMM.R
Q.EEMMRR(365)QQEGFKGTFPDAR(378)EQEIRMGQM.A
Precursor m/z: 764.71576, Charge: 3
Precursor m/z: 1149.2104, Charge: 3
Relative Abundance
Relative Abundance

Hu_FigS3

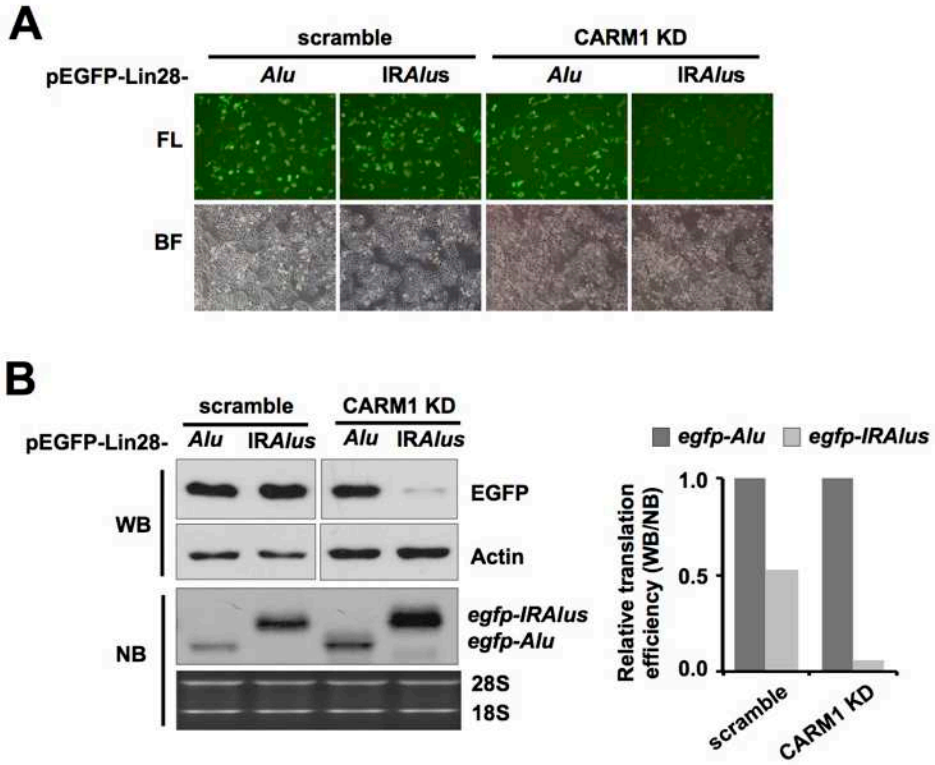
A
scramble
CARM1 KD
pEGFP-Lin28-
Alu
IRAlus
Alu
IRAlus
FL
BF
B
scramble
CARM1 KD
pEGFP-Lin28-
Alu
IRAlus
Alu
IRAlus
WB
NB
EGFP
Actin
egfp-IRAlus
egfp-Alu
28S
18S
egfp-Alu
egfp-IRAlus
Relative translation efficiency (WB/NB)
1.0
0.5
0.0
scramble
CARM1 KD

Hu_FigS4

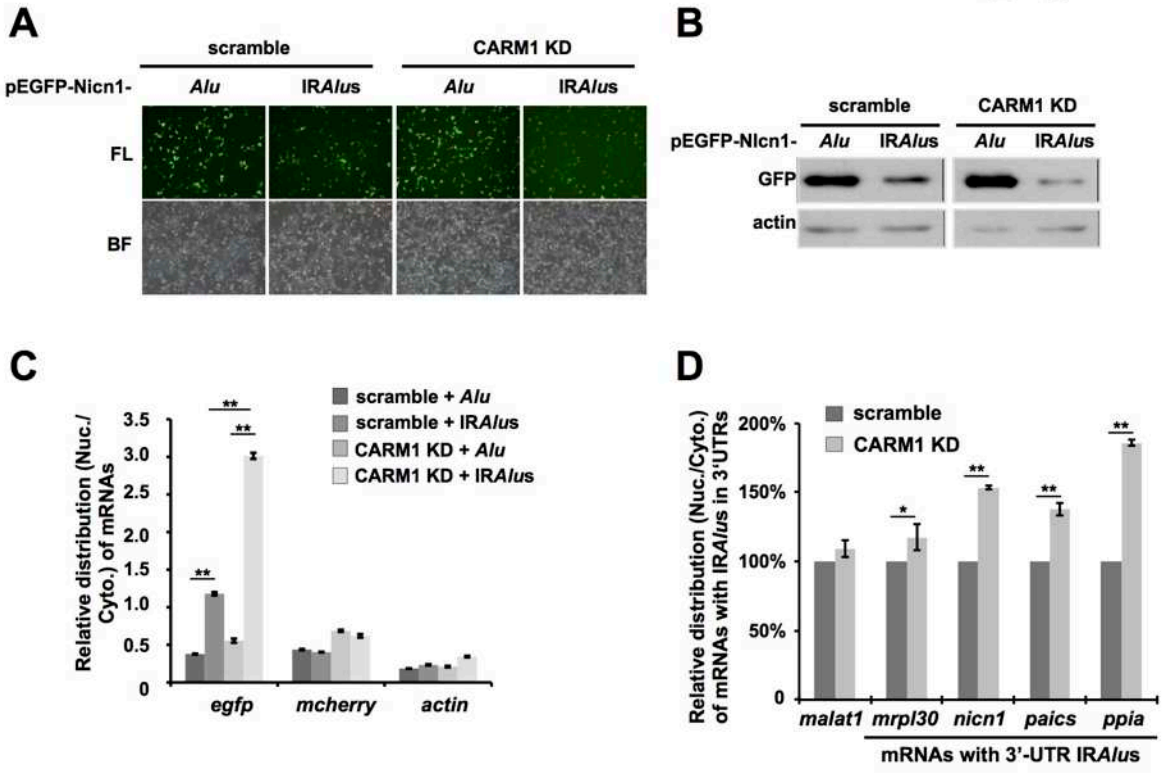
A
scramble
CARM1 KD
pEGFP-Nicn1-
Alu
IRAlus
Alu
IRAlus
FL
BF
B
scramble
CARM1 KD
pEGFP-NIcn1-
Alu
IRAlus
Alu
IRAlus
GFP
actin
C
scramble + Alu
scramble + IRAlus
CARM1 KD + Alu
CARM1 KD + IRAlus
Relative distribution (Nuc./Cyto.) of mRNAs
3.5
3.0
2.5
2.0
1.5
1.0
0.5
0
**
**
**
egfp
mcherry
actin
D
scramble
CARM1 KD
Relative distribution (Nuc./Cyto.) of mRNAs with IRAlus in 3'UTRs
200%
150%
100%
50%
0
*
**
**
**
malat1
mrpl30
nicn1
paics
ppia
mRNAs with 3'-UTR IRAlus

Hu_FigS5

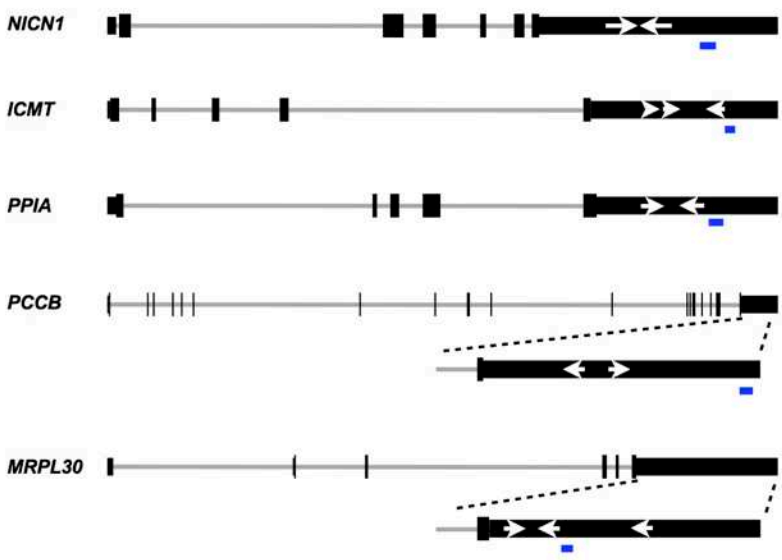

Hu_FigS6

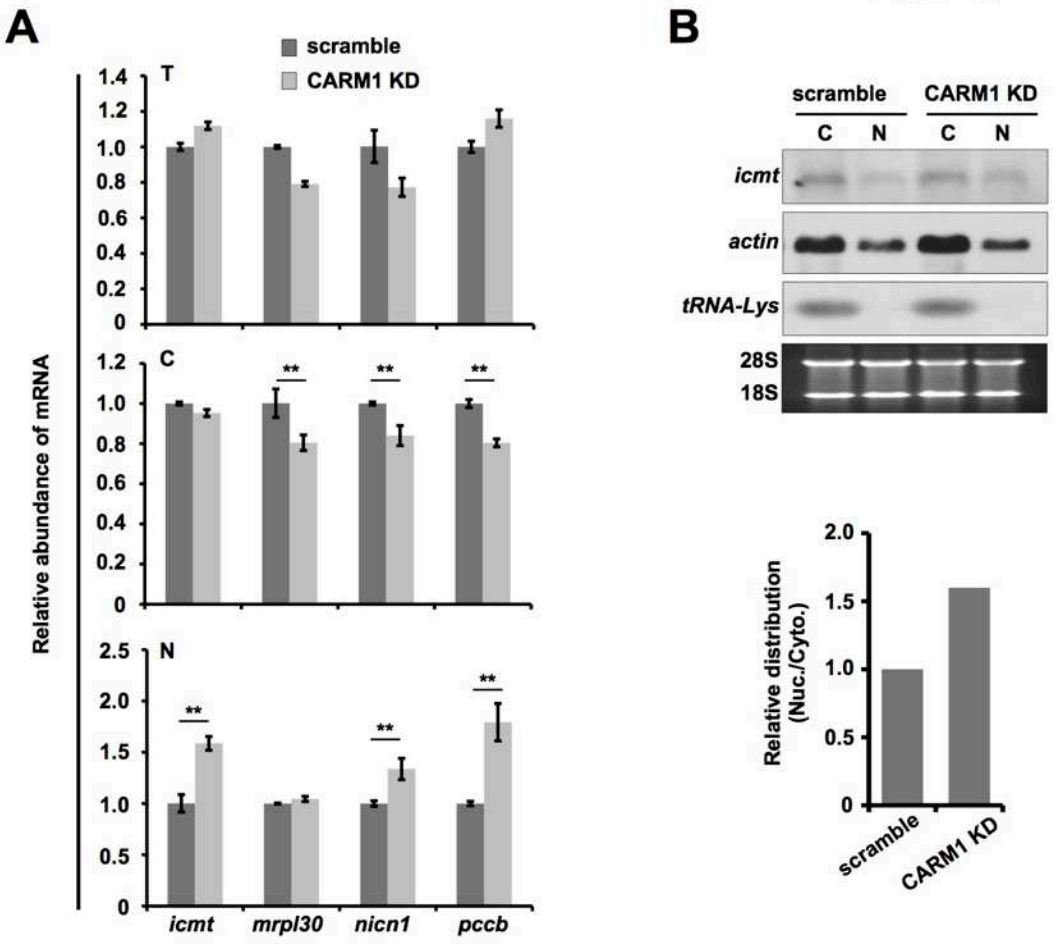
A
scramble
CARM1 KD
T
C
N
Relative abundance of mRNA
1.4
1.2
1.0
0.8
0.6
0.4
0.2
0
2.5
2.0
1.5
0.5
**
icmt
mrpl30
nicn1
pccb
B
scramble
CARM1 KD
C
N
icmt
actin
tRNA-Lys
28S
18S
Relative distribution
(Nuc./Cyto.)
scramble
CARM1 KD

Hu_FigS7

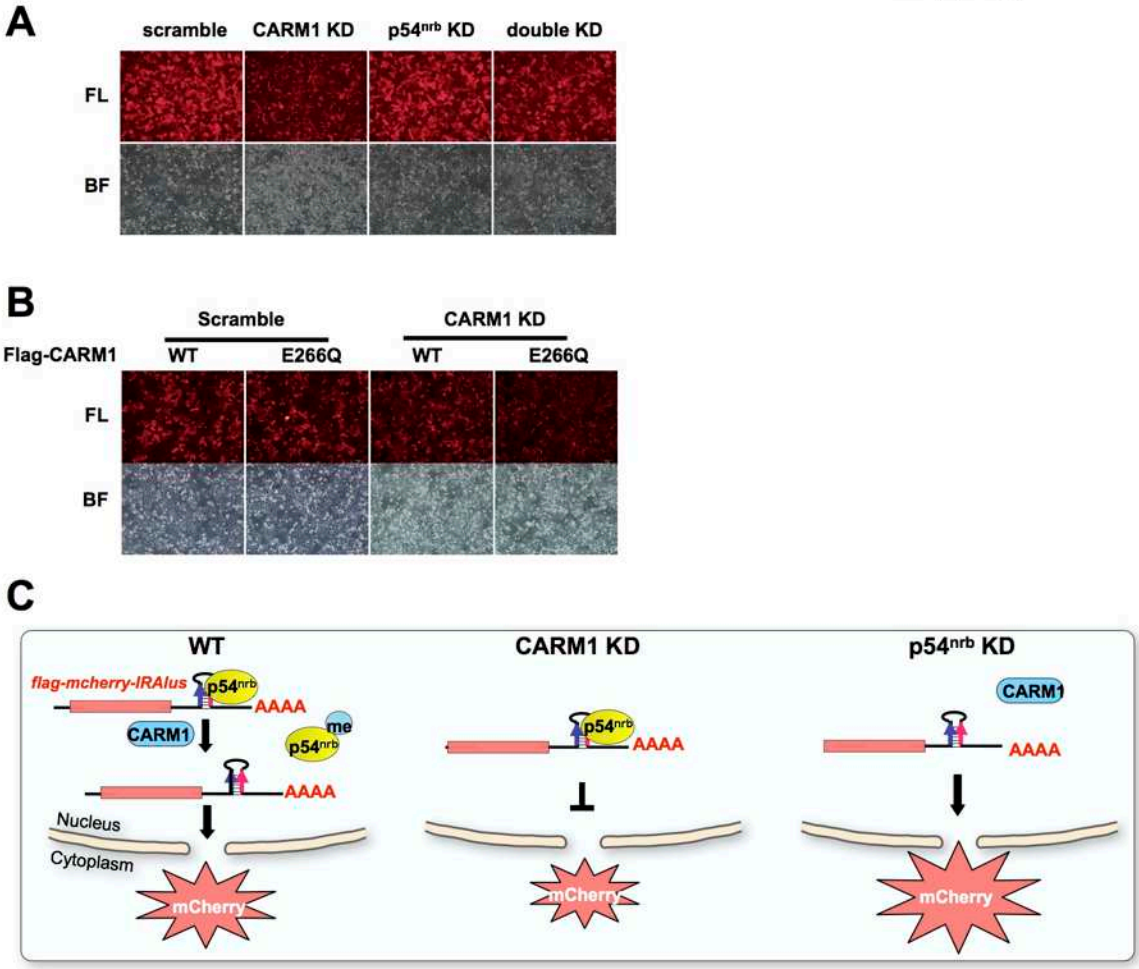
A
scramble
CARM1 KD
p54nrb KD
double KD
FL
BF
B
Scramble
CARM1 KD
Flag-CARM1
WT
E266Q
WT
E266Q
FL
BF
C
WT
CARM1 KD
p54nrb KD
flag-mcherry-IRAlus
p54nrb
AAAA
CARM1
me
p54nrb
AAAA
Nucleus
Cytoplasm
mCherry
p54nrb
AAAA
mCherry
CARM1
AAAA
mCherry

Supplemental Table S1. Primers used in this study.

qPCR primers for IRAlus Genes	
qNicn1-F	ACTTCATCTGCAAGGTCACTTAC
qNicn1-R	ACAGTAGTCTGTCCTCATGTGG
qPAICS-F	CGTAATTTTGGACTGCCACA
qPAICS-R	AGGTTTCATGGACAGCGAAC
qPccb-F	CGGTGTACAGCATCTGTTGG
qPccb-R	CATCTCTGCCAAAAACCACA
qMRPL30-F	GTGAGTGGCTCTTTGCATGA
qMRPL30-R	AGCTGGCATCCAGTGTTTCT
qICMT-F	CCTCACGAAAGGCTTCACTC
qICMT-R	GGCCACATCACCAATTTTCT
qPPIA-F	AGGGAAGCATATTGGGCTTT
qPPIA-R	CCTCTGCAGGGAGACTGACT

qPCR primers for NEAT1	
qNEAT1-F	TCGGGTATGCTGTTGTGAAA
qNEAT1-R	TGACGTAACAGAATTAGTTCTTACCA
qNEAT1-up-3F	GCAGTGATCAAACAAGGCTTC
qNEAT1-up-3R	TCAGTGTCCCTTAGGCTCAAA
qNEAT1-up-2F	ACGGCCTCTTCCCACTTAAT
qNEAT1-up-2R	AGGCATCGTGGTTTTGACTC
qNEAT1-up-1F	CAACAACATCCGGGAAGAAA
qNEAT1-up-1R	CAGTGTATCCCCGCTTCTCT
qNEAT1-1F	GGAGGGCCGGGAGGGCTAAT
qNEAT1-1R	CGGTCAGCCCCGTCGAGCTA
qNEAT1-2F	TCCTCCTGGTGGCCAAGACAGC
qNEAT1-2R	GCTAAGGGGCAGCGAAGGATGC
qNEAT1-3F	TTCTTCCCCTTTACAGCACA
qNEAT1-3R	TCGTTATGAAGGCAATGTGA
qNEAT1-4F	GCCACATTCTTTGCCTTCAT
qNEAT1-4R	CCCACACCTCTGGAAATTCA
qhNEAT1_2-F(qNEAT1-5F)	TGACTCTCCATTTCCCCATC
qhNEAT1_2-R(qNEAT1-5R)	TCATTTACCCGCATTTCACA
qNEAT1-6F	GCATTTTTCCTCTTTGACCA
qNEAT1-6R	GTGCTTTTTGCACCAACAAT
qhNEAT1_2-F-2(qNEAT1-7F)	TTGCAGCAACTGTCCTGAAG
qhNEAT1_2-R-2(qNEAT1-7R)	GGGTCCGGGATTATAGAGGA
qNEAT1-8F	GCCTGTTGTCCTTACACCAT
qNEAT1-8R	TAGGGCTTCCCTTCGCTATT
qNEAT1-9F	GGGGTGTCCCCTATCAGACT
qNEAT1-9R	AATGCTTTCCCATGATCCAG

qNEAT1-10F	GCCATCCGAGGAAGATGTAA
qNEAT1-10R	GGGATGTTGATGGAGTGACC
qNEAT1-11F	CCCACCTGGTAGTCCTCAGA
qNEAT1-11R	TGGGTGCCTTCTACTCATCC

Other qPCR primers	
qGFP-F	ACAAGCAGAAGAACGGCATC
qGFP-R	ACTGGGTGCTCAGGTAGTGG
qmcherry-F	CCCCGTAATGCAGAAGAAGA
qmcherry-R	GGCCTTGTAGGTGGTCTTGA
qhIFNβ-F	CAGCAGTTCCAGAAGGAGGA
qhIFNβ-R	AGCCAGGAGGTTCTCAACAA
qACTB-F	GGACTTCGAGCAAGAGATGG
qACTB-R	AGCACTGTGTTGGCGTACAG
qACTB for ChIP and NRO F	CCTCATGGCCTTGTCACACGAG
qACTB for ChIP and NRO R	GCCCTTTCTCACTGGTTCTCT
qnucleolin-F	CCTCAGCAAAGAAGGTGGTC
qnucleolin-R	GCCAGGTGTGGTAACTGCTT

Primers for NB probes	
F-Sp6-NICN1-upstream	GCGATTTAGGTGACACTATAGGACCTTTCCCAAG TGGCTCT
R-T7-NICN1-upstream	GCGTAATACGACTCACTATAGGGACCACTAGGGG ACACACAGG
F-Sp6-actin	GCGATTTAGGTGACACTATAGTGCTATCCCTGTAC GCCTCT
R-T7-actin	GCGTAATACGACTCACTATAGGGAGTACTTGCGC TCAGGAGGA
F-tRNA-Lys	GATCCGCCCGGATAGCTCAGTCGGTAGAGCATCA GCTTTTAATCTGAGGGTCCAGGG
R-tRNA-Lys	AGCTTCGCCCGAACAGGGACTTGAACCCTGGAC CCTCAGATTAAAAGTCTGATGCTCTA
F-NEAT1	GGGCCATCAGCTTTGAATAA
R-T7-NEAT1	TGAATTGTAATACGACTCACTATAGGGTCCCCATA CATGCGTGACTA

Biotin Pulldown primers	
F-T7-GFP	GCGTAATACGACTCACTATAGGGATGGTGAGCAA GGGCGAGGA
R-GFP	TTATCTAGATCCGGTGGATC
F-T7-dsEGFP	GCGTAATACGACTCACTATAGGGCACAAGTTCAG CGTGTCCG

R-T7-dsEGFP	GCGTAATACGACTCACTATAGGGGTTCACCTTGATGCCGTTC

Dig-RNA Pulldown primers	
F-T7-IR*Alu*s	GCGTAATACGACTCACTATAGGGCACGTGTCTCTAGCAAAACC
R-IR*Alu*s	ATGCTGAGCATATCTCTTGG

Plasmid	**Vector**	**Insert**	**Restriction enzyme**
pcDNA3.1(+)-flag	pcDNA3.1(+)	flag	HindII BamHI
pcDNA3.1(+)-flag-p54^{nrb}-wt	pcDNA3.1(+)-flag	full length p54^{nrb}	BamHI XhoI
pcDNA3.1(+)-flag-p54^{nrb}-mut	pcDNA3.1(+)-flag	R357,365,378K mutation of p54^{nrb}	BamHI XhoI
pcDNA3.1(+)-flag-EGFP	pcDNA3.1(+)-flag	EGFP	BamHI XhoI
pTracer-CARM1-WT	pTracer	WT CARM1	EcoRI NotI
pTracer-CARM1-E266Q	pTracer	E266Q mutation of CARM1	EcoRI NotI
pmCherry-flag-IR*Alu*s	pmCherry-C1	IR*Alu*s from pEGFP-C1-Nicn1-IR*Alu*s	EcoRI XhoI
pcDNA3.1(+)-flag-p54^{nrb}-1	pcDNA3.1(+)-flag	1-230bp of p54^{nrb}	BamHI XhoI
pcDNA3.1(+)-flag-p54^{nrb}-2	pcDNA3.1(+)-flag	54-375bp of p54^{nrb}	BamHI XhoI
pET28a-p54^{nrb}	pET28a	full length	BamHI EcoRI
pET28a-p54^{nrb}-△1	pET28a	1-89bp of p54^{nrb}	BamHI EcoRI
pET28a-p54^{nrb}-△2	pET28a	90-131bp of p54^{nrb}	BamHI EcoRI
pET28a-p54^{nrb}-△3	pET28a	132-226bp of p54^{nrb}	BamHI EcoRI
pET28a-p54^{nrb}-△4	pET28a	227-309bp of p54^{nrb}	BamHI EcoRI
pET28a-p54^{nrb}-△5	pET28a	310-361bp of p54^{nrb}	BamHI EcoRI
pET28a-p54^{nrb}-△6	pET28a	362-471bp of p54^{nrb}	BamHI EcoRI
pET28a-p54^{nrb}-R357,365K	pET28a	R357,365K mutation of p54^{nrb}	BamHI EcoRI
pET28a-p54^{nrb}-R378,383K	pET28a	R378,383K mutation of p54^{nrb}	BamHI EcoRI